Near-substrate gradients in chain relaxation and viscosity in a model low molecular weight polymer

Tamanna Rahman[a] and David S. Simmons[b*]

[a] Department of Polymer Engineering, The University of Akron, Akron, Ohio 44325, United States

[b] Department of Chemical, Biological, and Materials Engineering, University of South Florida, Tampa, Florida 33620, United States

KEYWORDS Glass transition, molecular dynamics, interfacial gradients, nanoconfinement, nanorheology

ABSTRACT: Polymers in the nanoscale vicinity of interfaces can exhibit large alterations in dynamics and glass formation behavior. These changes are accompanied by alterations in rheological response, yet the precise nature of gradients in viscosity and whole-chain relaxation near interfaces is an open question. Here we employ molecular dynamics simulations of a low molecular weight glass-forming polymer between crystalline walls to probe this relationship. Results indicate that viscosity and whole-chain relaxation time gradients for this system obey the same qualitative phenomenology as do segmental relaxation time gradients, indicating that they emanate from the same underlying physics. At a quantitative level, however, our simulation and theoretical results indicate that unlike in small molecules, polymer viscous and whole chain relaxation interfacial gradients should generally be expected to be weaker than underlying segmental relaxation time gradients – a consequence in large part of the typically weaker bulk temperature dependence of low-temperature viscosity and whole chain relaxation than segmental dynamics in many polymers. Shifts in viscosity are shown to emerge from underlying alterations in the polymer's complex modulus near interfaces, with a high-frequency glassy plateau emerging at higher temperature and surviving to lower frequency near the walls. These results have implications for the rheological response of diverse nanostructured polymers including thin films, filled rubber, ionomers, and semicrystalline polymers, and they highlight the need for a generalization of the Rouse model to account for dynamical gradients.

Introduction

Extensive evidence indicates that polymers in the nanoscale vicinity of interfaces can exhibit large changes in dynamics and glass formation behavior[1–5]. Examples include freestanding polymer films, supported polymer films[6,7], semicrystalline polymers[8,9], ionomers[10–12], nanocomposites, and block copolymers[13–17]. Study of these effects has in most cases focused on intrinsically segmental phenomena such as segmental relaxation and the glass transition temperature T_g. Simulations and experiments point to large (up to 50 K or more) shifts in T_g in material $<$ 10 nm from an interface with large accompanying shifts in relaxation times[18–20].

Results over the last decade have led to a reasonably coherent picture of the phenomenology of segmental relaxation time gradients near interfaces[1]. The form of these gradients can be understood at two deeply-connected levels. The bulk relaxation time is recovered double-exponentially with increasing distance z from the interface[4,21–28]:

$$\tau(z,T) = \tau_{bulk}(T)\exp\left[-A(T)\exp\left(-\frac{z}{\xi_{\ln\tau}(T)}\right)\right], \quad (1)$$

where τ is the relaxation time, τ_{bulk} is the bulk relaxation time, $A(T)$ quantifies the temperature-dependent fractional reduction in the quantity $\ln(\tau/\tau_{bulk})$ immediately at the interfaces, and $\xi_{\ln\tau}$ is the exponential decay range for recovery of bulk-like relaxation times. This functional form is underpinned by a more fundamental exponential variation of the activation barrier for relaxation, i.e.[1,28,29]

$$\gamma(z) - 1 \equiv \frac{\Delta F(z,T)}{\Delta F_{bulk}(T)} - 1 = (\gamma_0 - 1)\exp\left(-\frac{z}{\xi_F}\right), \quad (2)$$

where $\gamma(z)$ -1 is the fractional change in the local activation barrier $\Delta F(z,T)$ relative to its bulk value $\Delta F_{bulk}(T)$ at a distance z from the interface, γ_0 is the fractional reduction at the interface, and ξ_F is the range for recovery of bulk-like activation barriers.

Crucially, the range parameter ξ_F has been found to be temperature-invariant at sufficiently low temperatures – a reflection of the remarkable finding that the local activation barrier in thin films can be factored into distinct position-dependent and temperature-dependent factors[1,28,29]:

$$\Delta F(z,T) = \gamma(z)\Delta F_{bulk}(T). \quad (3)$$

This fact leads to a fractional power law relationship between local or confined dynamics at bulk dynamics at low temperatures[1,28,29]:

$$\frac{\tau(z,T)}{\tau_{bulk}(T)} = \left(\frac{\tau_{bulk}(T)}{\tau^*}\right)^{\gamma(z)-1}, \quad (4)$$

where τ^* is a chemistry- and relaxation-function-dependent bulk relaxation timescale of onset of strong interfacial effects on dynamics, such that dynamics are nearly bulk-like at temperatures for which the bulk relaxation time is less than this value[29,30].

The theoretical understanding of this phenomenology has also advanced during this time. A recent perspective paper on the state of theoretical progress in this area[1], coauthored by one of us, reviewed a number of theoretical efforts to understand these effects and concluded that the Elastically Cooperative Nonlinear Langevin Equation (ECNLE) theory of supercooling liquid dynamics[31,32] has been shown to predict essentially the full segmental-level phenomenology of near-interface gradients described above[28]. Within this theory, interfacial gradients in segmental dynamics are predicted to emerge from a combination of altered near-interface segmental caging constraints and a longer-range alteration of a collective elastic activation barrier to relaxation. The decoupling relation above is predicted by ECNLE to emerge from the close connection between these two effects, such that the net truncation in activation barrier at any position (z) is nearly temperature-invariant.

In addition to the ECNLE theory, several other theoretical proposals have also been found to be consistent with elements of the above phenomenology, including the fractional power law decoupling relation. For example, the cooperative free volume model of Lipson and coworkers has recently been shown to be consistent with the fractional power law decoupling relation[33]. Therefore, at present there is at least one near complete theoretical prediction of interfacial gradients in segmental relaxation time (the ECNLE theory), with several other promising approaches that may ultimately prove to offer alternative theoretical descriptions of the scenario with further development.

In any case, practically, as a consequence of the empirical success and theoretical rationality of equation (4), it is possible to extract the local fractional alteration $\gamma(z)$-1 in the activation barrier from local and bulk relaxation time data.

In parallel to the gradual development of this cohesive picture of interfacial gradients in segmental dynamics, there has been considerable interest in alterations in effective viscosity and rheological response of glass-forming polymers near interfaces. At the very small length scales associated with these effects, it is not clear that viscosity is perfectly well-defined in the bulk sense[34]. Nevertheless, prior work has reported alterations in rheological response that can be readily described based on altered effective viscosities defined in the normal manner based on a ratio between shear stress and strain rate[34–39].

Indeed, multiple experimental studies have suggested that rheological response properties near interfaces exhibit alterations of a magnitude at least reasonably according with observed alterations in T_g and segmental dynamics. Dewetting experiments by Tsui and coworkers[35] probed viscosity in thin films, reporting substantial reductions in viscosity with decreasing film thickness. Film x-ray photon correlation spectroscopy measurements have likewise reported suppressed viscosities in supported (free-surface-dominated) films[36]. By using a film-step deformation method, Chai et al. reported more locally on near-free-surface viscosities and demonstrated substantial reductions relative to bulk.[37] Experiments probing the leveling of surface dimples[38] or the embedding of particles into film surfaces[40–42] have yielded similar findings. The most recent of work in this area has directly visualized nanoscale *gradients* in experimental polymer viscosity near a free surface[39]. These types of shifts also likely play a central role in the 'bound rubber' phenomenon wherein mechanical response is argued to be altered in the nanoscale vicinity of nanoparticulate additives in rubber[43–47].

A series of studies by McKenna and coworkers has probed creep of freestanding films via a nanobubble inflation method[48–51]. These studies have reported a series of intriguing findings wherein the *rubbery modulus* of the polymer can be enhanced even when T_g is decreased. Moreover, the timescale of relaxation of the rubbery plateau in these films seems is found to vary quite differently in distinct polymers, in various cases appearing to be either longer- or shorter-lived in the bulk. These findings indicate the potential for nontrivial differences between alterations in T_g and alterations in chain relaxation in thin films. However, their interpretation is complicated by the fact that these polymers are highly entangled. It is thus possible that topological entanglements effects[52,53] may play a role, even if they do not provide the full picture. An understanding of the underlying effect of the interfacial T_g gradient on rheological response in the absence of potential confounding entanglement effects will require study of rheological response in unentangled systems, which is likely not possible via bubble inflation at temperatures appreciably above T_g.

Multiple simulation studies have reported results consistent with altered effective viscosity near interfaces in glass-forming polymers. Early simulation work by Varnik and Binder directly reported a gradient of enhanced viscosity in a bead-spring polymer under Poiseuille flow near an attractive substrate[54]. Results by Priezjev suggest that this basic phenomenon persists under Couette flow, with simulated polymers in this scenario exhibiting a growing near-wall region of reduced shear rate (and thus enhanced effective local viscosity) as density is increased towards vitrification[55]. The fact that qualitatively similar effects are seen in these two types of flow suggests that, at a minimum, trends in effective nanoscale viscosity are *qualitatively* transferrable between distinct flow types. Servantie and Müller likewise reported simulation evidence for a domain of altered viscosity in polymers near a wall, with this effect driving modified effective slip length[34]. Simulations of Lam and Tsui[56] and by our group[39] indicate that an inverse phenomenon occurs at free surfaces, where viscosity is locally reduced.

A natural question is whether these alterations obey the same phenomenology as do segmental relaxation time alterations near interfaces. Given that gradients in rheological response are the direct determinant of many of the performance properties of interfacially rich polymers, the need to extend the understanding of segmental-scale gradients to this larger molecular scale is a major open challenge in the area.

Indeed, despite the now fairly advanced understanding of the phenomenology of segmental relaxation time gradients, it remains unclear precisely how alterations in polymer viscosity and mechanical response shifts emerge from those gradients in more local dynamics. In small molecules, viscosity is directly connected to the glass transition, since each molecule effectively consists of a single 'segment' and the viscosity is therefore directly connected to the segmental alpha relaxation process. In polymers, on the other hand, the situation is more complicated. Viscosity is most directly connected in polymers to whole chain motion rather than segmental motion. The classical model connecting motion at these two scales in polymers is the Rouse theory, which is grounded in the assumption that segmental relaxation times are uniform across the entire system[57]. Near interfaces, this assumption is evidently violated, such that the Rouse description cannot be assumed to hold.

Moreover, the connection between viscosity and segmental dynamics is imperfect even in the bulk state of glass-forming polymers: polymer viscosity is commonly observed to exhibit a weaker temperature dependence than polymer segmental dynamics[58]. There is considerable debate over the origins of this decoupling[58–60]. One body of literature suggests that it is grounded in the emergence of spatially heterogeneous dynamics on cooling[58,61,62], while several other perspectives argue for an origin that is unrelated to dynamic heterogeneity.[63–67] Regardless, however, of the full explanation for this decoupling phenomenon, recent work by our group extending the Rouse model to account for a distribution of segmental relaxation times indicates that, as a general matter, non-uniform segmental mobility should be expected to drive a breakdown of the standard Rouse scaling of dynamics[61]. If bulk dynamic heterogeneity can lead to breakdown in the Rouse model far from interfaces, one might expect this breakdown to occur in an even more extreme manner near interfaces. Moreover, there the situation is even more complicated: not only does the system possess a distribution of relaxation times, but this distribution is spatially organized due to the presence of a dynamical gradient upon approach to the interface.

Given this situation, it is not at all clear whether gradients in polymer viscosity at interfaces should closely reflect gradients in segmental dynamics. Similarly, it is not clear whether gradients in other rheological response functions, such as the complex modulus, should directly follow segmental relaxation time gradients. No present generalization of the Rouse model accounts for strong, spatially correlated variations in segmental mobilities as are present in these systems. Given that chain motion reflects mobility over a larger scale than does segmental motion, one might anticipate some degree of attenuation of the mobility gradient as probed by viscous rather than segmental response.

With these issues in mind, here we seek to answer the following questions with respect to rheological gradients near interfaces:

1) Do gradients in whole chain relaxation time and polymer viscosity obey the same *qualitative* phenomenology summarized above for segmental relaxation time gradients – exponential barrier gradients, double-exponential viscosity gradients, and fractional power law decoupling?
2) To what extent do gradients in chain relaxation time and viscosity *quantitatively* reflect underlying gradients in segmental relaxation?
3) How do these gradients reflect underlying gradients in the complex modulus of the polymer?

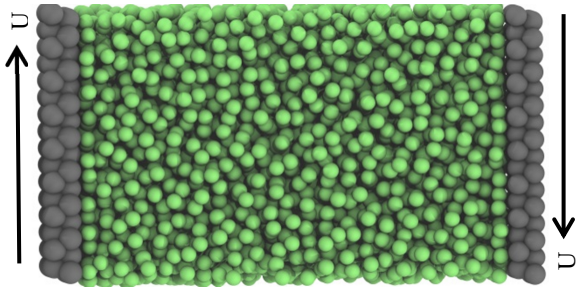

Figure 1. Simulation snapshot (rendered in VMD) illustrating geometry of simulated system, with polymer beads in green and wall beads in grey.

Here we seek to answer these questions in the context of flexible, unentangled, short-chain polymers at a rigid substrate. To do so, we perform molecular simulations of a flexible bead spring polymer in a gap between two crystalline substrates. We focus on a case in which polymer-wall interactions are slightly stronger than polymer-polymer interactions, leading to a large near-wall T_g enhancement. At a very coarse qualitative level, this suggests that our system is more akin to poly(methyl methacrylate) on silica (where T_g is enhanced near the substrate) than polystyrene on silica (where near-substrate effects on T_g are relatively muted. We probe both equilibrium gradients in dynamics for both segments and whole chains, and gradients in local viscosity under Couette flow conditions.

Methods

Simulation methodology

We perform equilibrium and nonequilibrium molecular dynamics simulations probing relaxation dynamics and rheological response in the vicinity of a polymer-substrate interface. Simulations employ an attractive variant of the standard bead-spring model of Kremer and Grest[68], which has been extensively employed to study near-interface dynamics during glass formation[19,39,69–79]. Within this model, the non-bonded fluid monomer interaction is governed by the Lennard-Jones (LJ) potential:

$$V_{LJ}(r) = 4\varepsilon\left[\left(\frac{\sigma}{r}\right)^{12} - \left(\frac{\sigma}{r}\right)^{6}\right] . \quad (5)$$

The LJ potential is truncated for $r \leq r_c = 2.5\sigma$. $\varepsilon = 1$ and $\sigma = 1$ set the characteristic energy and length scales, respectively, for nonbonded interactions. In addition to the LJ potential, any two covalently neighboring monomers in the chain interact through the Finitely Extensible Nonlinear Elastic (FENE) potential:

$$V_{FENE}(r) = \frac{1}{2}KR_0{}^2 ln\left[1-\left(\frac{r}{R_0}\right)^2\right] + 4\varepsilon\left[\left(\frac{\sigma}{r}\right)^{12} - \left(\frac{\sigma}{r}\right)^6\right] + \varepsilon, \quad (6)$$

with the values for the parameters K=30εσ^{-2}, R_o=1.3σ, ε = 1 and σ = 0.8. We use these modified values of the parameters of the FENE model to prevent heterogeneous nucleation and crystallization under nanoconfinement by rigid crystalline walls[80].

A layer of polymer approximately 23 segmental diameters thick is sandwiched between two structured crystalline walls, modeled by two layers of beads of FCC lattice with density of 1.4. The 111 face of the lattice is exposed inward towards the polymer film. Periodic boundary conditions are employed in all directions. A simulation snapshot (rendered in VMD[81]) illustrating the system geometry is shown in Figure 1.

Equilibrium configurations of the simulated samples over a range of temperatures are obtained in an iterative manner by the Predictive Stepwise Quenching (PreSQ)[82] algorithm. In summary, we first anneal the samples at a high temperature, T=1.5, which is much greater than the glass transition temperature. The system, equilibrated at this high temperature, is then quenched to 8 evenly spaced temperatures high enough that the expected relaxation time is less than 1 ps. Each of these configurations is then annealed for a period of 10 ps. Data are collected from subsequent runs, and a relaxation time τ for each temperature is determined in the manner described below. The determined equilibrium temperature vs τ data are then fit to the Vogel-Fulcher-Tammann (VFT) relation and extrapolated over a range of 0.5 to 1 order of magnitude further in relaxation time projecting 8 new evenly spaced temperatures over that relaxation time range. These temperatures are then isothermally annealed for at least 10 times their end-to-end reorientational relaxation time. The process of rapid quenching and VFT fitting is iterated to obtain new equilibrated system configurations at the new subsequent lower temperatures until a target maximum whole chain relaxation time is reached.

Simulations are performed in LAMMPS[83] at a constant pressure P = 0, by employing the Nose-Hoover barostat as implemented in LAMMPS, with a damping parameter of 2 τ_{LJ}. Temperature in quiescent simulations is controlled with the Nose-Hoover thermostat, also with a damping parameter of 2 τ_{LJ}. Temperatures during shear are controlled with the Berendsen thermostat after performing a brief additional equilibration in the Berendsen thermostat.

Results are reported in dimensionless Lennard-Jones units. Roughly, one LJ unit of time τ_{LJ} corresponds to one picosecond in real units. There is no unique conversion of length units to real units, but a typical range is one LJ length unit σ_{LJ} to 0.5 to 2 nm[13,71,84]. Similarly, there is no general temperature scale conversion, but a conversion of 1 LJ temperature unit to 1000K yields a temperature scale comparable to typical room temperature glassy polymers such as polystyrene. With these figures in mind, a dimensionless velocity of 1 corresponds approximately to 10^3 m/s.

Quantification of dynamics

Translational dynamics are quantified via the self-part of the intermediate scattering function,

$$F_s(q,t) = \left\langle \frac{1}{S}\sum_k^S \frac{1}{N}\sum_j^N \left\{\exp\left[-i\boldsymbol{q}\cdot\left(\boldsymbol{r}_j(t+s_k) - \boldsymbol{r}_j(s_k)\right)\right]\right\}\right\rangle_{|\boldsymbol{q}|=q}, \quad (7)$$

where $\boldsymbol{q}$ is a wavevector corresponding to wavenumber q, $\boldsymbol{r}_j(t)$ is the position of particle j at time $t+s$, s_k is a start time of observation, N is the number of particles in the system, S is the number of observation windows averaged over, and the brackets denote an average over numerous wavevectors corresponding to wavenumber q. We compute $F_s(q,t)$ at q = 7.07, comparable to the first peak in the structure factor. This calculation is performed at two levels: for single beads, and at the level of the center of mass of each entire chain. To do the latter, we first compute the center of mass of each chain and when then apply equation (7) at the level of this center of mass, consistent with recent work employing this method[61].

In analyzing this relaxation function, the Kohlrausch−Williams−Watts stretched exponential fit is employed for data smoothing and interpolation,

$$F_s(q,t) = hexp\left[-\left(\frac{t}{\tau_{KWW}}\right)^{\beta}\right] \quad (8)$$

where τ_{KWW} is a time constant, h is called the non-ergodicity parameter, and β is the stretching exponent. The segmental relaxation time τ_α is defined as the time at which F_s(q,t) decays to 0.2, following a convention commonly employed in simulations[61,72,79,85].

Reorientational relaxation is quantified via the reorientational autocorrelation function $C_2(t)$, given by

$$C_2(t) = \langle P_2[e_i(0).e_i(t)]\rangle, \quad (9)$$

where P_2 is the second Legendre polynomial and $\boldsymbol{e}_i(t)$ is the i'th unit vector under consideration at time t. We again compute this quantity at both a segmental and whole chain dynamics. For whole chain dynamics, we employ the end-to-end vector of the chain. Since for single segments (n=1), there is no internal vector within this model, we employ the bond vector between adjacent bonded beads. Like translational relaxation time, the reorientational relaxation time is also defined when this relaxation function decays to 0.2 after employing a stretched exponential fit for smoothing and interpolation.

At each temperature, gradients in translational dynamics and reorientational dynamics are computed via the self-part of the intermediate scattering function (at a wavenumber comparable to the first peak in the structure factor) and the second Legendre polynomial vector reorientation function, respectively. For segmental translational dynamics, the gradient is obtained by sorting beads (segments) into bins of thickness 0.875 and computing F_s(q,t) for particles within each bin. For whole chain translational dynamics, chain centers of mass are instead sorted into these bins. For reorientational dynamics, a bond or end to end vector is sorted into a bin based on the position of the midpoint of the vector.

Quantification of spatially-resolved rheological response

In addition to these quiescent analyses, the system is separately, at each temperature, subjected to shear to obtain a viscosity and complex modulus.

Viscosity is obtained via simulations in which we translate the upper wall at a fixed velocity of U and the lower wall at a fixed velocity of -U. We employ a standard value of U $=0.001\ \sigma_{LJ}/\tau_{LJ}$. Below, we establish the range of conditions in which this value of U is in the linear regime, by varying U in a set of initial probe runs.

Viscosity gradients are obtained in a manner paralleling recent nanorheology experiments and simulations[39], via differentiation of the displacement gradient within a lubrication approximation after steady state is achieved. Specifically, the velocity $u_x(z)$ within each bin is first determined by computing the incremental displacement of beads within that bin. Time intervals are chosen to generate 2000 data points per simulation run. Incremental displacements are summed to calculate the total displacement as a function of time. The velocity in a given bin is then obtained from the slope of the fit to the displacement vs time curves beyond the point where the system reaches steady state (i.e. beyond the point at which the displacements become linear in time). The resulting velocity profile is then converted to a viscosity profile $\eta(z)$ via the equation

$$\tau_{xz} = \eta(z)\frac{du_x(z)}{dz}\ , \qquad (10)$$

where τ_{xz} is the shear stress and is computed for the film from LAMMPS, in a manner comparable to recent work[39]. The shear stress is averaged over the same period of time used to obtain the velocity gradient from local displacements (i.e. after displacement vs time curves are linear and the system has reached steady state).

To extract the storage and the loss modulus, oscillatory motion is imposed on the polymer layer by imposing a sinusoidal displacement on the walls in the direction parallel to the film. The displacement $X(t)$ of the upper wall is given in the equation

$$X_w(t) = X_0\sin(\omega t), \qquad (11)$$

where X_0 sets the amplitude and ω the frequency of the oscillatory wall displacement. The lower wall is displaced in opposite direction with equal amplitude and frequency. Generally 20 to 100 cycles are performed in order to obtain sufficient data while maintaining tractable relaxation times.

In order to obtain a spatially resolved complex modulus from these runs, the shear stress is first extracted in a spatially-resolved layer-wise manner from LAMMPS for layers of thickness Δz. The time interval of reporting is chosen such that 50 data points per cycle of oscillation are generated, and the stress is averaged over the interval between points. The stress response $\sigma(t,z)$ for each layer of the polymer is then fit to a sinusoidal function with stress amplitude, σ_0, frequency, ω and a phase lag δ_σ.

$$\sigma(t,z) = \sigma_0(z)sin(\omega t + \delta_\sigma(z)) \qquad (12)$$

The mean displacement, $X(z,t)$ is then obtained for layers ('bins') of fluid, with the bins used for displacement calculations shifted by Δz/2 such that the locations at which

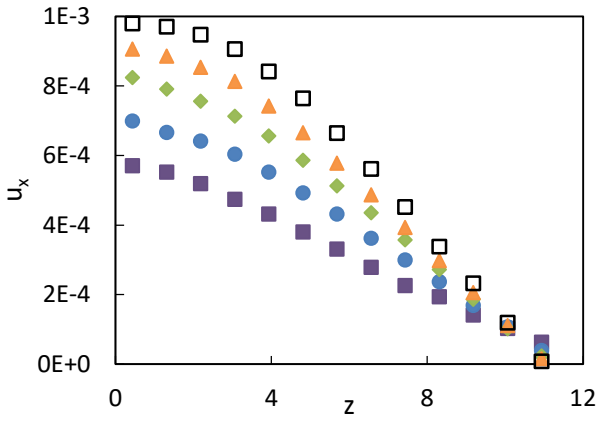

Figure 2. Velocity vs position profiles for representative temperatures of 0.810 (purple squares), 0.693 (blue circles), 0.615 (green diamonds), 0.567 (orange triangles), and 0.496 (open squares). These temperatures correspond to (bulk-like) mid-film segmental reorientational relaxation times of 14, 29, 60, 116 τ_{LJ} (corresponding roughly to ps in real units), respectively.

stress and displacement are computed are staggered. The local strain γ(t,z) is then computed as

$$\gamma(t,z) = \frac{dX(z,t)}{dz} \qquad .(13)$$

Because these strain derivatives are centered between each pair of adjacent bins of particles for which displacement was computed, the computed strain values reflect a set of mean positions corresponding with the mean positions at which stress was computed. The magnitude of the strain wave, γ_0 is extracted by fitting the strain data, calculated from displacement of each layer, to a sinusoidal wave function as.

$$\gamma(t,z) = \gamma_0(z)\sin(\omega t(z)+\delta_\gamma(z)). \qquad (14)$$

The loss modulus, G' and storage modulus, G" are then calculated using the equations

$$G' = (\sigma_0/\gamma_0)\cos(\delta) \qquad (15)$$

and

$$G" = (\sigma_0/\gamma_0)\sin(\delta) \qquad ,(16)$$

where δ is the phase lag between streess and strain and computed by substracting δ_γ from δ_σ. As described further below, the viscoelastic linear regime of the system at a given frequency is identified by checking if the moduli are independent of strain-rate by using multiple strain amplitude at constant frequency.

Results

Linearity

As shown by representative velocity vs position curves in Figure 2, steady state velocity profiles are nonlinear in position, as expected, indicating a spatial variation in shear rate and thus in viscosity. At higher temperatures, there is appreciable temperature-dependent slip at the walls, consistent with prior work[34]. The true system shear rate, if measured between the first layers of the fluid on each side of the gap, is therefore temperature dependent. In reporting data, we refer to given conditions based on a nominal mean

shear rate define as twice the wall velocity over the distance between walls. However, the *viscosity* calculation above is insensitive to these issues within the linear regime, because it employs *local* rather than global strain rates. Wall slip effects thus generally do not impact local viscosity determinations provided that the response is in the linear regime.

We thus begin by assessing the question of whether our results for viscosity reflect linear regime behavior. To do so, we report in Figure 3a the ratio of local viscosities at a nominal strain rate of $9x10^{-4}$ to those at a strain rate of $9x10^{-5}$, corresponding to wall velocities 0.01 and 0.001. A ratio of 1 in this figure indicates that viscosity is insensitive to shear rate, pointing to linear behavior in this range of shear rates. In Figure 3b, we plot the ratio of near-wall to midfilm viscosity at multiple shear rates. Here, agreement of multiple data sets (multiple shear rates) indicates linearity. As can be seen here, the midfilm viscosity remains approximately linear down to the lowest temperatures probed in the study, while the layer nearest the wall remains approximately linear down to a temperature of 0.54 for shear rates less that $9x10^{-4}$ and a temperature of 0.49 for shear rates less that $9x10^{-5}$. The loss of linearity at higher temperature near the surface than in the mid-film can be understood at a coarse level via the view that near-substrate polymer is effectively shifted to a higher "rheological temperature"[86] than the bulk-like polymer in the mid-film. We discuss further the origins of this behavior from the standpoint of complex modulus further below. For now, we note that in the ensuing analysis we employ viscosity data only at conditions where Figure 3 and the associated analysis indicate that the viscosity reflects linear behavior.

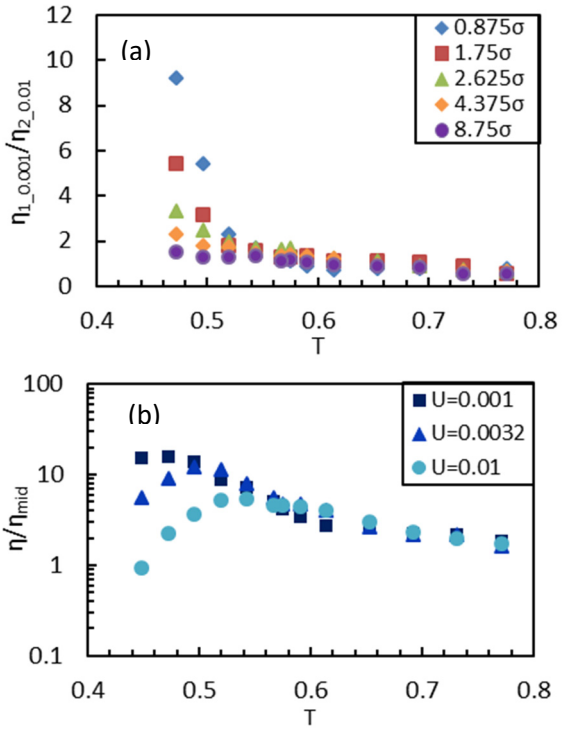

Figure 3. (a) Ratio of viscosity measured at wall velocities of 0.001 and 0.01 (corresponding to nominal overall shear rates of 9×10^{-4} and 9×10^{-5}, respectively, at distances from the wall noted in the caption, as a function of temperature. (b) Near-wall viscosity measured at the three noted wall velocities, corresponding to nominal overall shear rates of $9x10^{-4}$, $3x10^{-4}$ and $9x10^{-5}$, from top to bottom, plotted versus temperature.

Viscosity and relaxation time gradients

We continue by assessing the form of these linear-regime viscosity gradients and of the underlying gradients in whole-chain relaxation. We initially ask whether they obey the double-exponential form for recovery of bulk-like behavior observed for segmental relaxation time gradients. To do so, we first select several representative temperatures and in Figure 4 depict a double-log plot of segmental and whole chain relaxation time gradients vs distance from the interface for relaxation times (translational and reorientational for segments and whole chains) and viscosity gradients. As can be seen here, all of these gradients obey a double-exponential recovery of bulk-like behavior with increasing distance from the interface, such that they obey equation (1) or its viscosity analogue. Evidently, segmental dynamics, whole chain dynamics, and viscous response in these low molecular weight chains exhibit qualitatively comparable behavior near a substrate.

We note that in performing fits to equation (1) and generally in normalizing results by bulk throughout this study, we employ the approximation that $\tau_{mid} \cong \tau_{bulk}$ and $\eta_{mid} \cong \eta_{bulk}$. Equation (1), together with prior evidence, indicates that this is a reasonable approximation in our system, where the midline is approximately 10σ from the interface. Prior work has reported that, near attractive supporting substrates, ξ in these equations is ~2 or less[21,22,87]. Below we report values of this range parameter that are consistent with this finding. With this range value, the residual deviation from bulk of τ and η at the midplane is 5% or less, even when the near-interface dynamics differ from bulk by a factor of 1000 (larger than the largest effect we observe in this study). Deviations from bulk of this magnitude are within the noise of relaxation time determinations and will only matter if analyzing normalized properties in the high-z tail of this gradient – an issue we do not address here.

Next, we ask whether alterations in the *temperature dependence* of whole-chain relaxation and viscosity near the interface qualitatively mirror the fractional power law rule (equation (4)) seen in segmental dynamics. If so, this will enable extraction of γ(z) (the position-dependent activation barrier modification factor) and thus enable a test of the underlying exponential variation in activation barriers. To test this, we plot in Figure 5 local values of each relaxation time and of viscosity vs their mid-film values.

As can be seen in this figure, at low temperatures all five relaxation processes obey equation (4) near the substrate. The *onset* behavior of equation 4 is nonuniform across the 5 relaxation functions, with viscosity exhibiting a more pronounced onset than the other four. In prior work, we explored this onset behavior for segmental translation and reorientation at a *free surface* across a matrix of bead-

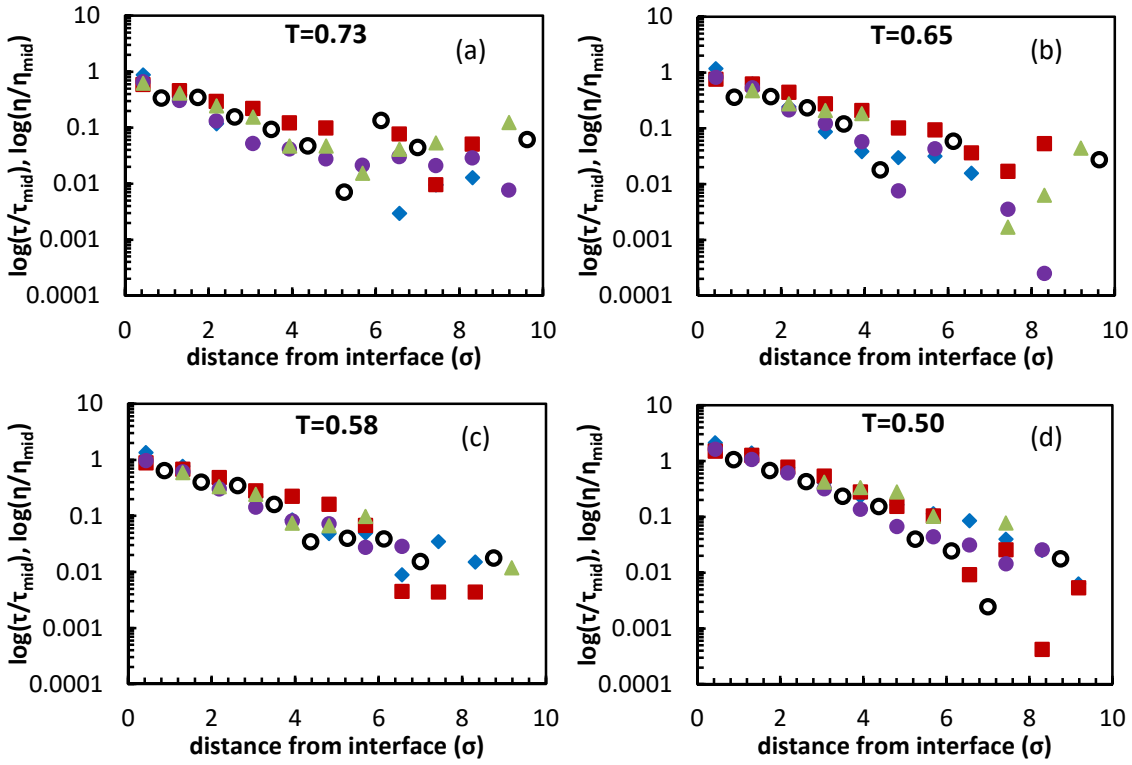

Figure 4: Normalized viscosity (black hollow circles) and relaxation times for translational segmental dynamics (blue diamonds), translational whole chain dynamics (red squares), reorientational segmental dynamics (purple circles), reorientational whole chain dynamics (green triangles) as functions of distance from interface at reduced LJ temperatures of (a) 0.73, (b) 0.65, (c) 0.58 and (d) 0.50. For context, these temperatures correspond to (bulk-like) mid-film segmental reorientational relaxation times of 22, 40, 102 and 530 τ_{LJ} (corresponding roughly to ps in real units), respectively.

spring polymers and found that the timescale of the onset can vary with chemistry and even with relaxation function at fixed chemistry[30]. Similarly, we found variation in the 'sharpness' of the onset, with bulklike behavior recovered very abruptly at high temperature in some relaxation functions and more gradually in others. In the present case, it appears that the onset behavior is more pronounced (at perhaps at larger effective timescales) in the viscous response relative to segmental and chain relaxation times, with a well-defined high-temperature regime in which effects are quite weak followed by onset of much stronger effects at lower temperature.

Evidently, both the form of the gradient in ln(τ) or ln(η) and the temperature dependence of these gradients obey a qualitatively common phenomenology across all of these relaxation functions. By employing fits of the data in Figure 5 to equation (4), we can now additionally ask whether the exponential recovery of bulk-like activation barriers that *underlies* equation (1) for segmental dynamics is also obeyed by chain relaxation and viscosity.

As in our prior work[29,30], we constrain our fit to equation (4) to low temperatures, only, in an effort to avoid contamination by data below or within this onset. The fit range associated with each quantity is shown in the rightmost column of Table 1. As shown in Figure 6a, the decay of γ-1 (i.e. the fractional enhancement in activation barrier) can indeed be described by an approximately exponential form (equation (2)) with distance from the interface for all relaxation functions probed.

Magnitude and range of relaxation time and viscosity gradients

The above findings suggest that the phenomenology of gradients in whole-chain relaxation and viscosity *qualitatively* parallel that of segmental relaxation: all obey a double-exponential recovery of bulk relaxation times with increasing depth in the film, reflecting an underlying exponential gradient of the activation barrier, and obeying a fractional power law decoupling relation with the corresponding bulk dynamics as temperature is varied at low temperature. To what extent are these gradients in whole chain relaxation and viscosity in *quantitative* agreement with the corresponding segmental gradients as well?

In answering this question, we must consider two gradients for each relaxation function: the gradient in ln(τ) or ln(η), which obeys a double-exponential recovery of bulk with increasing distance from the interface, and the gradient in the activation barrier underlying each relaxation process, which obeys a single-exponential recovery of bulk with increasing distance from the interface. These two gradients are characterized by a total of four figures of merit. $A(T)$ and γ_0 quantify the magnitude of surface alterations in $\ln(\tau/\tau_{bulk})$ (or $\ln(\eta/\eta_{bulk})$) and in $\Delta F/\Delta F_{bulk}$, respectively. $\xi_{ln\tau}(T)$ and $\xi_{\Delta F}$ report on the exponential decay range for

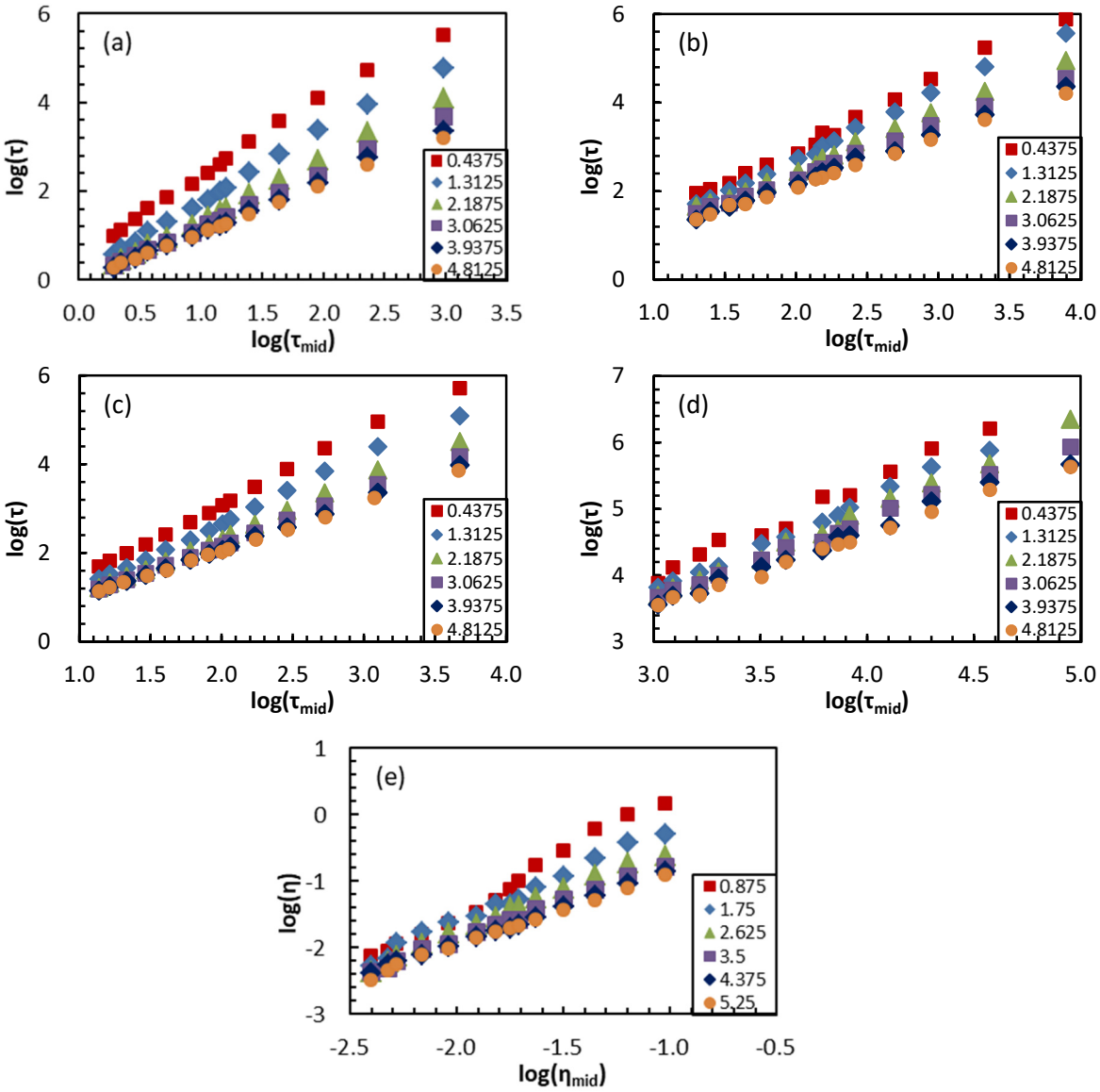

Figure 5: (a) Segmental translational relaxation time, (b) whole chain translational relaxation time, (c) segmental reorientational relaxation time, (d) whole chain reorientational relaxation time and (e) viscosity, all vs their corresponding values in the middle of the film, plotted for layers of thickness 0.875 at the indicated mean distances from the wall. Typical standard deviation in log(τ) or log(η), computed by averaging over the two halves of the film immediately at the substrate, are 0.01 (segmental translation), 0.05 (whole chain translation), 0.01 (segmental reorientation), 0.04 (whole chain reorientation), and 0.05 (viscosity).

recovery of bulklike $\ln(\tau/\tau_{bulk})$ (or $\ln(\eta/\eta_{bulk})$) and bulk activation barrier, respectively. Before examining the quantitative behavior of each of these gradients in our simulated system, it is useful to consider the manner in which we should *expect* them to interrelate.

First, if we combine equations (1) and (2) with a generalized activation rate law,

$$\tau(T,z)=\tau_0\exp\left[\Delta F(T,z)/kT\right], \quad (17)$$

applied both locally and at a whole film level, we arrive at the finding that the fractional surface reduction $A(T)$ of the $\ln(\tau/\tau_{bulk})$ gradient must be related to the fractional reduction in activation barrier at the interface via the equation

$$A(T)=\gamma_0\,\Delta F_{bulk}(T)/kT \quad (18)$$

A parallel finding for free surface behavior was discussed in recent work[1]. This equation indicates that the fractional surface reduction $A(T)$ of $\ln(\tau/\tau_{bulk})$ and $\ln(\eta/\eta_{bulk})$ gradients should grow on cooling even when the magnitude γ_0 of the underlying activation barrier gradient is temperature invariant (as the success of equation(4) at low T indicates) – a consequence of a growing *bulk* activation barrier, relative to the thermal energy, on cooling.

Notably, equation (18) can also be rewritten as

$$A(T)=\gamma_0\ln\left(\frac{\tau_{bulk}(T)}{\tau_{0,bulk}}\right), \quad (19)$$

where $\tau_{0,bulk}$ is the prefactor in the bulk activation rate law. We thus generally expect larger magnitude gradients in $\ln(\tau/\tau_{bulk})$ or $\ln(\eta/\eta_{bulk})$ for relaxation functions that exhibit a stronger temperature dependence in bulk.

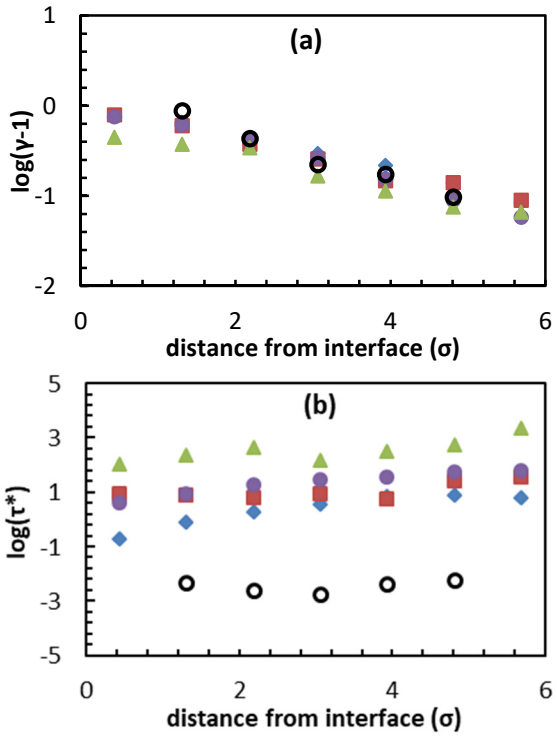

Figure 6: (a) Logarithm of fractional activation barrier enhancement and (b) logarithm of onset timescale τ^* or onset viscosity η^* as functions of distance from the interface for translational segmental (blue diamonds), translational whole chain (red squares), reorientational segmental (purple circles), and orientational whole chain (green triangles) relaxation times and viscosity (black open circles).

With this expected behavior in mind, we quantify the magnitude of alterations in $\ln(\tau)$ and $\ln(\eta)$ and their underlying activation barriers in the simulated system. As can be seen in Figure 7a, the fractional surface reduction $A(T)$ of $\ln(\tau/\tau_{bulk})$ and $\ln(\eta/\eta_{bulk})$ for all four of the relaxation times probed grow with cooling. As discussed above, this growth can be attributed to the development of the *bulk* relaxation time for each relaxation function on cooling, as per equations (18) and (19). The absolute value of these interfacial alterations in relaxation time or viscosity varies among the relaxation functions. As seen in this figure, segmental translation is most strongly perturbed at the interface, with whole chain reorientation exhibiting the weakest. Gradients in viscosity, whole chain translational relaxation, and segmental reorientation exhibit intermediate surface amplitudes.

This relaxation-function-to-function variation in $A(T)$ can be compared with the variation in the surface magnitude γ_0 of alterations in the activation barriers underlying these relaxation processes. As seen in Table 1, γ_0 is smallest for whole-chain reorientation, consistent with the trend for $A(T)$. The values of γ_0 for the other three relaxation functions (excluding viscosity) are not distinguishable within uncertainty. However, remarkably, γ_0 for viscosity is by far the largest of any of the relaxation functions, which would seem to presage large interfacial modifications in $\ln(\eta)$; however, this is not consistent with the findings in Figure 7a, which indicate a relatively weak ln(η) gradient.

In essence, these findings indicate that alterations to the activation barrier for viscosity very near the substrate are relatively large on a fractional basis, and yet alterations to the actual viscosity itself are relatively weak. How can these findings be consistent? To understand this, we turn again to equation (19), which indicates that the strength of temperature dependence of the *bulk* relaxation time for viscosity plays a critical role in mediating between the strength of barrier gradients and the strength of gradients in $\ln(\tau)$ or $\ln(\eta)$. To assess if this factor can account for the apparent discrepancy between the strength of $\ln(\eta)$ gradients and the underlying barrier gradients, we plot in Figure 8 the mid-film temperature dependences of viscosity and the five relaxation times considered here. As can be seen in this figure, viscosity indeed exhibits an anomalously low bulklike temperature dependence as compared to the other four relaxation times considered, predicting the lower ratio of $A(T)/\gamma_0$ observed above.

This finding may have broad implications for the understanding of altered dynamics under nanoconfinement. Equations (18) and (19) indicate that, *even given a comparable alteration in activation barriers*, larger alterations should be expected in the dynamics of chemistries and relaxation function exhibiting a stronger bulk temperature dependence. However, this strength of temperature dependence is not the *only* factor controlling the strength of these interfacial gradients – the interfacial barrier reduction factor γ_0 plays a separate role that does not necessarily involve a dependence on the strength of the temperature dependence of dynamics.

This result may rationalize the findings that the strength of interfacial effects on T_g often[20], but not always[70,76,88], correlates with the fragility of glass formation – a measure of the strength of the temperature dependence of dynamics near T_g. However, the *mechanism* is quite different than has often been proposed in prior works, which have commonly attributed this correlation to a putatively larger correlation

Table 1. Surface magnitude γ_0 and exponential decay range ξ_F of alterations in the activation barriers underlying viscosity and the four relaxation times considered here: translational segmental relaxation time, translational whole-chain relaxation time, reorientational segmental relaxation time, and reorientational whole-chain relaxation time. The rightmost column provides the midfilm timescale range over which fits to equation (4) were performed. Fits to equation (2) are performed over the range $z < 4$ to avoid contamination by noisier data at higher z. Uncertainty intervals are 95% confidence intervals on the parameters for the fit.

Relaxation function	$\gamma_0 - 1$	$\xi_{\Delta F}$	Fit range
η	2.50 ± 0.69	1.26 ± 0.36	$\eta_{mid} > 0.015$
$\tau_{\alpha,t}$	0.81 ± 0.28	2.66 ± 0.94	$\tau_{\alpha,t,mid} > 10$
$\tau_{wc,t}$	0.85 ± 0.21	2.23 ± 0.50	$\tau_{wc,t,mid} > 100$
$\tau_{\alpha,r}$	1.04 ± 0.57	1.97 ± 0.85	$\tau_{\alpha,r,mid} > 100$
$\tau_{wc,r}$	0.54 ± 0.12	3.29 ± 0.96	$\tau_{wc,t,mid} > 1000$

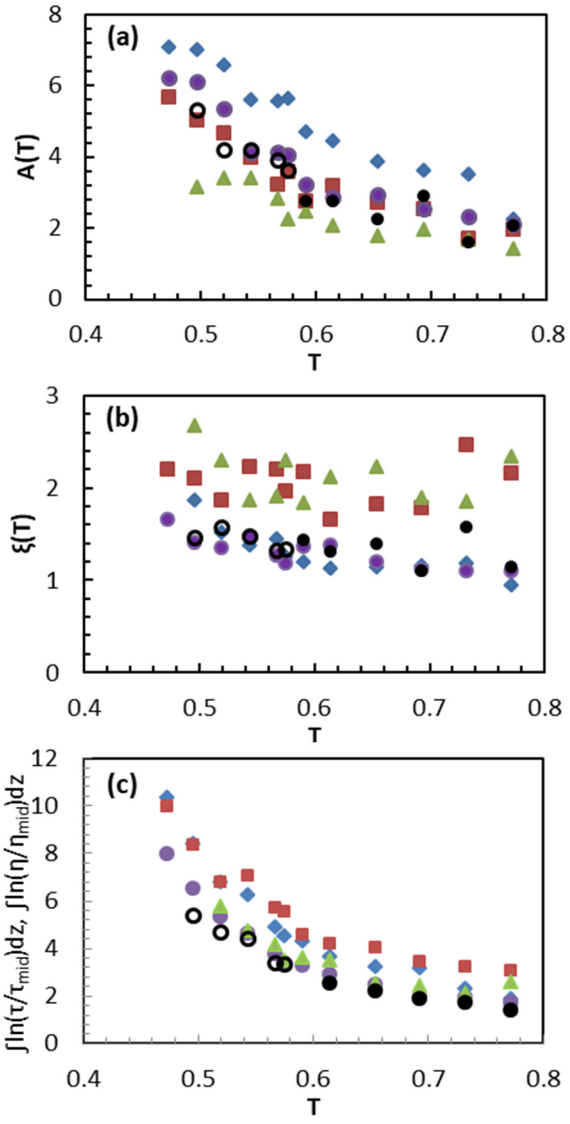

Figure 7: (a) Surface magnitude, (b) range and (c) integrated magnitude of interfacial perturbations to translational segmental relaxation (blue diamonds), translational whole chain relaxation (red squares), reorientational segmental relaxation (purple circles), and reorientational whole chain relaxation (green triangles) viscosity (black open circles at wall velocity of 0.001 and closed circles at a higher wall velocity of 0.01.)

length scale in more fragile glass-formers. Instead, we find that this result emerges at a more physically trivial level from a simple convolution of a relatively uniform activation barrier gradient with distinct bulk temperature dependences of dynamics.

This finding also points to a likely molecular weight dependence of the strength of viscosity gradients as compared to segmental relaxation time gradients. In small molecules, molecular relaxation and viscosity are relatively well coupled. However, in polymers, this coupling can break down, with viscosity and whole-chain relaxation often reported to exhibit a weaker temperature dependence than segmental relaxation[58,61,61,65,89–96]. As indicated above, this weaker temperature dependence leads to a lower magnitude surface modification in viscosity relative to

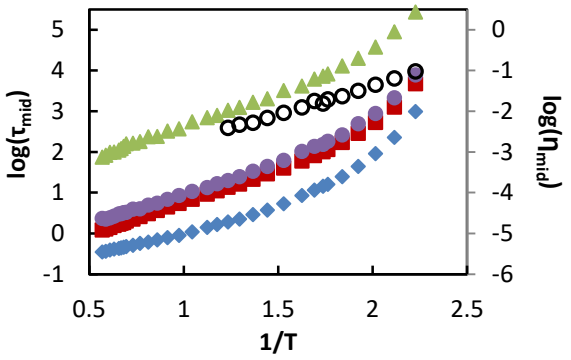

Figure 8. Logarithmic viscosity (black hollow circles) and relaxation times for translational segmental dynamics (blue diamonds), translational whole chain dynamics (red squares), reorientational segmental dynamics (purple circles), reorientational whole chain dynamics (green triangles), plotted vs inverse temperature. Viscosities at the temperatures above the glass formation range are not reported due to excessive noise.

segmental relaxation time. Since the coupling between viscosity and segmental relaxation must be restored as the polymer chain molecular weight is reduced towards the small molecule limit, this implies that viscosity gradients should strengthen (relative to segmental relaxation time gradients) at low molecular weights. Because quite low molecular weights are needed to restore segmental-chain dynamical coupling[92], we expect that this trend should only become evident in the oligomer limit.

Further quantitative insight into the extent of the difference in strength in viscosity and segmental relaxation time gradients can be obtained by combining equation (19) with the experimental observation that, at low temperatures, the relationship between viscosity and segmental relaxation time is itself described by a fractional power law[58,91],

$$\frac{\eta_{bulk}(T)}{\tau_{\alpha,bulk}(T)} = a\left(\tau_{\alpha,bulk}(T)\right)^{-\varepsilon_{\alpha-\eta}} \quad (20)$$

where $\varepsilon_{\alpha-\eta}$ is a segment-viscosity decoupling exponent, a is a prefactor, and subscript α denotes the segmental process. Combination of this equation with equation (19) leads to the result that the difference between the segmental gradient magnitude $A_\alpha(T)$ and the viscosity gradient magnitude $A(T)$ at low temperature (where prefactor effects can be neglected) is given by the equation

$$A_\alpha(T) - A_\eta(T) \cong \varepsilon_{\alpha-\eta}\ln\left(\frac{\tau_{\alpha,bulk}(T)}{\tau_{0,bulk}}\right) - \left(1-\varepsilon_{\alpha-\eta}\right)\left(\gamma_{\eta 0}-\gamma_{\alpha 0}\right)\ln\left(\frac{\tau_{\alpha,bulk}(T)}{\tau_{0,bulk}}\right) \quad (21)$$

Here the first term reflects differences in gradient strength resulting from bulk decoupling between segmental dynamics and viscosity; the second term reflects differences resulting from differences in the underlying barrier gradient. The findings above suggest that, at least in these simulations, the first term plays a major role. Notably, $\varepsilon_{\alpha-\eta}$ or its equivalent for segment vs chain relaxation decoupling are available or can be readily obtained for a range of

polymer liquids (commonly ranging from 0 to ~0.6)[58]. Equation 20 suggests that this exponent is a predictor of the strength of viscosity gradients near interfaces, with higher values of $\varepsilon_{\alpha-\eta}$ presaging weaker interfacial viscosity gradients, given similar temperature-dependences of segmental dynamics. This finding may guide selection of glass-forming liquids with relatively uniform viscosity near interfaces.

We next turn to the question of the gradient range. As shown by Figure 7b, the range of $\ln\tau$ and $\ln\eta$ gradients is relatively insensitive to temperature as compared to their magnitude, consistent with reports focused purely on segmental dynamics[25,26]. Particularly given this situation, combination of equations (1) and (2) suggests that $\xi_{\Delta F} \cong \xi_{\ln\tau}$, with some differences between the two expected due to the weak spatial variation in of the prefactor τ_0 in equation (17) (or equivalently of the constant τ^* in equation (4))[29], which is visible in Figure 6b. In general, uncertainties in $\xi_{\Delta F}$ in these data are fairly large due to the derivative nature of this quantity. Broadly, however, comparison of this length scale with $\xi_{\ln\tau}$ between Table 1 and Figure 7b suggests that these length scales are generally comparable, consistent with the expectation above.

Notably, both the relaxation time and activation barrier gradient range data are consistent in indicating that the range of the gradient in dynamics at a substrate is considerably less than that at a free surface. Both Table 1 and Figure 7b are consistent with an interfacial gradient of exponential decay range around 2. By contrast, simulations at free surfaces have indicated that the decay range there is about twice as large[25,26,29,30]. This is consistent with prior work suggesting an asymmetry in the range of dynamical gradient at free surfaces vs buried substrates[1]. Recent experimental work has also observed this asymmetry between the range of the gradient at buried interfaces for which T_g is decreased (longer range) vs increased (shorter ranged)[97–99], suggesting that interfacial T_g enhancements may generally propagate further into a materials than T_g suppressions.

These findings are also consistent with predictions of the ECNLE theory for thin film dynamics. The general range of segmental relaxation time gradients – around 2 σ – is in reasonable accord with ECNLE predictions of the range of segmental ln(τ) gradients near a structured substrate[87]. That theory also predicts the asymmetry between substrates and free surfaces, capturing the longer range observed at a free surface. Within the ECNLE theory, near-interface changes in dynamics are fundamentally driven by changes in local segmental caging and in a long-ranged elastic activation barrier for relaxation. The present findings thus would appear to be potentially consistent with that scenario.

Beyond this comparison to free surfaces, it is informative to compare the gradient range between distinct relaxation functions. Both $\xi_{\ln\tau}$ (or $\xi_{\ln\eta}$) and $\xi_{\Delta F}$ data are consistent with the observation of longer ranged gradients for whole chain reorientational relaxation than for segmental relaxation. This is consistent with the intuition that whole chain relaxation gradients at an interface might be somewhat 'smeared out' relative to segmental gradients due to intra-chain averaging. Gradients in the viscosity and in its underlying barrier are relatively short ranged, and more similar to that of segmental than whole chain dynamics, as per Table 1 and Figure 7b. This finding seems surprising, as viscosity is normally associated with whole chain motion. This unexplained observation emphasizes the need for an extension of the Rouse model to treat chain motion and viscous relaxation in a gradient of segmental mobilities.

From a practical standpoint, the depth-variation in $\ln\eta$ is more important than the depth-variation of the underlying barrier (because it more directly controls rheological

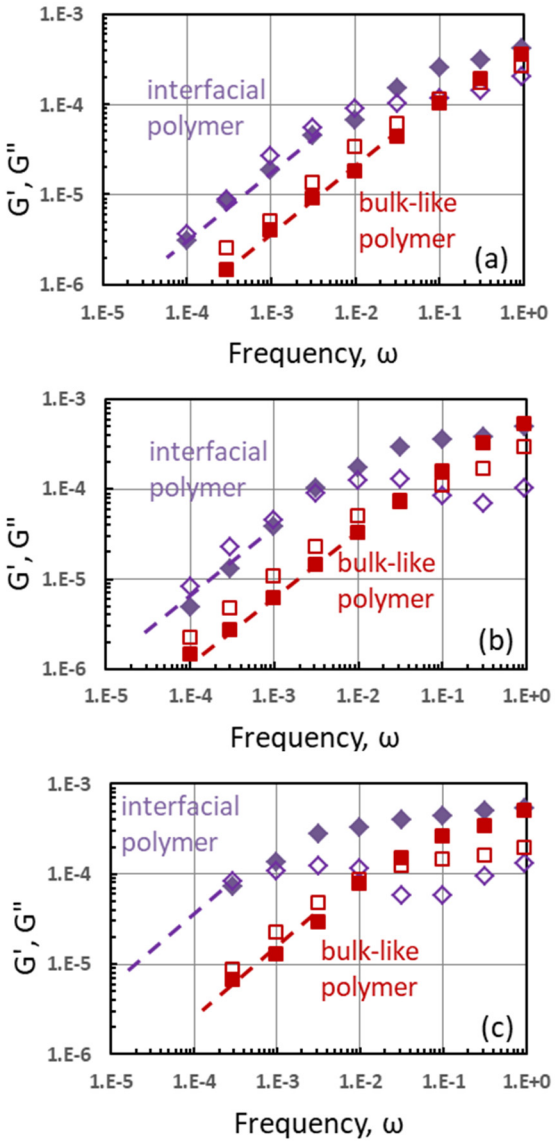

Figure 9: G' (solid symbols) and G" (unfilled symbols) vs ω at the interface (purple) and midfilm (red) for (a) T=0.59, (b) T=0.54 and (c) T=0.49, corresponding to mid-film segmental reorientational relaxation times of 82, 172, and 530 τ_{LJ}, respectively. Dotted lines denote the Rouse regime. In part (c), the location of the interfacial Rouse regime is an estimate as only the high frequency shoulder of the Rouse regime is within the accessible frequency range.

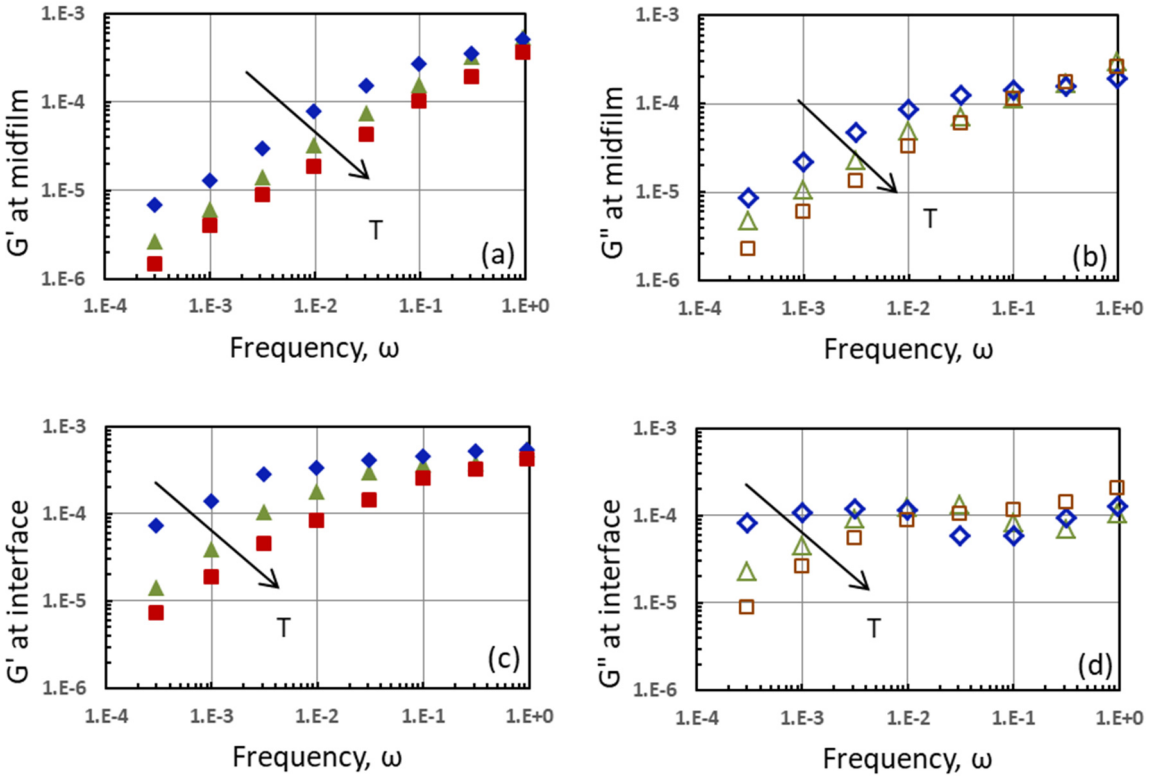

Figure 10: G' and (b) G" at mid-film and (c) G' and (d) G" at interface as function of ω for equilibrium temperature, T=0.49 (blue diamond), T=0.54 (green triangle) and T=0.59 (red square). These temperatures correspond to mid-film segmental reorientational relaxation times of 530, 172, and 82 τ_{LJ}, respectively.

response), and we thus focus on the implications of this aspect of the results. To do so, we quantify the *cumulative magnitude* of alterations in τ or η (not simply at the surface but integrated across the whole gradient) by calculating the numeric integral of $\ln(\tau/\tau_{mid})$ or $\ln(\eta/\eta_{mid})$ over the whole film. This quantity, shown in Figure 7c, can be interpreted as the *total* amount of 'extra' $\ln\tau$ or $\ln\eta$ near the interface. This quantity also has the advantage of reduced sensitivity to noise due to its direct integral (and non-fit) nature. Consistent with exhibiting both a low range and magnitude of $\ln\eta$ gradients, the integrated magnitude of the near-interface viscosity perturbation is the weakest of the functions probed here. These findings, together with those above, reinforce that alterations in polymer viscosity near interfaces should be expected to be relatively weaker than those in segmental dynamics, while still obeying a comparable *qualitative* phenomenology.

Complex modulus

Finally, in order to gain more insight into interfacial gradients in viscosity in particular, we probe gradients in complex modulus near the interface. The viscosity and the relaxation times are intimately connected to the complex modulus G(ω), since viscosity is the time integral of the relaxation modulus $\eta = \int_0^\infty G(t)dt$, and the complex modulus is the Fourier transform of the relaxation modulus – we thus expect that alterations in viscosity near the interface should be undergirded by alterations in complex modulus.

To proceed, we first perform oscillatory shear simulations at multiple strain amplitudes at each frequency. We use these amplitude sweeps to identify the linear regime amplitude in each frequency range. The data conforming to linearity are presented in Figure 9; data in this figure thus include multiple strain amplitudes to maintain linearity across the 4-decade frequency range probed without losing signal strength (simulated signal to noise ratios in simulated shear experiments can be unacceptably poor at excessively low amplitudes, so the best data are generally obtained at the highest possible amplitude that remains in the linear regime).

In Figure 9, G' and G" at interface are compared to their values in the midfilm as a function of frequency for three different reduced Lennard Jones temperatures: 0.59, 0.54 and 0.49. Results clarify the mechanical origin of linear enhancement in viscosity at the interface. At the highest temperature probed, which is only modestly below the onset of non-Arrhenius segmental dynamics, G' and G" exhibit a clear Rouse regime (slope ~ ½) in both the near-interface and mid-film dynamics. However, the Rouse regime is shifted ~1 decade to lower frequencies near the interface at this highest temperature. With decreasing temperature, the Rouse regimes in both domains shift to lower frequency as a result of a growing segmental relaxation time. However, the effect is evidently larger near the interface. At the lowest temperature of 0.49, the interfacial Rouse regime is shifted nearly out of the accessible frequency range. Based on the shoulder of the

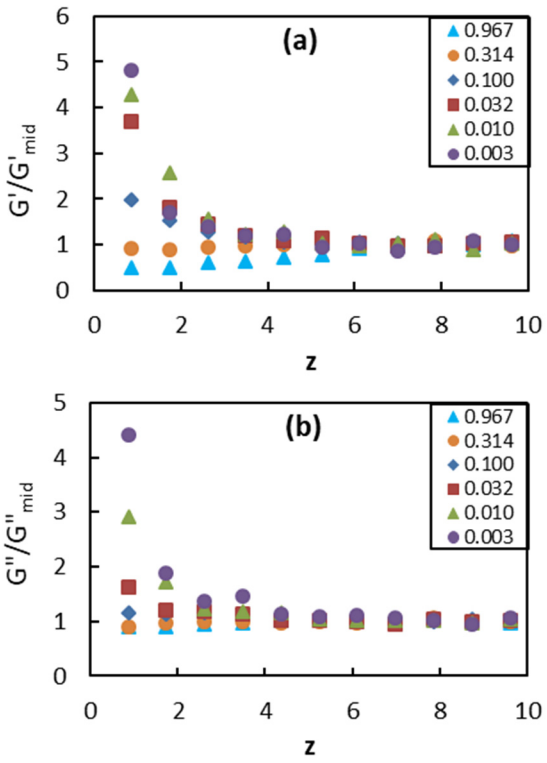

Figure 11. (a) G' and (b) G" gradients at a representative temperature 0.59 (corresponding to a segmental reorientational relaxation time of 82 τ_{LJ}. The symbols represent results for strain frequencies shown in the legend, normalized by their values in the midfilm. Results are at a fixed shear amplitude of 0.088.

Rouse regime visible near the interface, it is clear at this temperature that there is at least a ~2 decade difference in the interfacial and mid-film Rouse regimes observed at this temperature, and possibly more. This finding is consistent with and underlies the growing magnitude of the interfacial gradient in viscosity observed upon cooling in Figure 7.

In addition to the evident shift in the Rouse regimes near the interface and upon cooling, Figure 9 points to a related feature of the mechanical response near the wall: a well-established glassy plateau emerges in G' sooner near the wall than in the bulk. This trend can be seen more easily in Figure 10a, where these data are regrouped to place multiple temperatures in the same figure. In the midfilm at high temperature, the data lack any signature of a glassy plateau in G'(ω). This is a reflection of the fact that, at $T = 0.59$, the segmental α relaxation is not yet well-separated from the picosecond β relaxation at shorter times. Upon cooling, a soft glassy plateau of reduced slope begins to emerge in the mid-film. These findings are paralleled by results for G" in Figure 10b: there is a lack of any minimum in G" at high temperature, with a hint of an emerging minimum at the lowest temperatures.

This gradual emergence of a glassy plateau is greatly enhanced near the wall, as shown in Figure 10c and d. As can be seen here, by the lowest temperature probed the wall exhibits a well-established glassy plateau at high frequency in G', with a commensurate minimum in G". These findings indicate that the near-wall material is 'glassier' than the bulk, with slower alpha relaxation, a shift in the Rouse regime to lower frequency, and a better developed glassy plateau.

Finally, we directly consider in Figure 11 gradients in G' and G" through the film over a range of frequencies, at a fixed strain amplitude of 0.088. As can be seen here, both G' and G" exhibit a strong enhancement near the interface at low frequency. With increasing frequency, however, this effect weakens, and even inverts: at the highest frequencies probed, G' is reduced rather than enhanced at the interface. We emphasize that, unlike in Figure 9 and Figure 10, these data are at fixed amplitude and thus include nonlinear effects. The lowest frequency shown is in the linear response regime; at fixed amplitude, linearity is lost with increasing frequency, such that the effects observed at high frequency are nonlinear response effects. These findings hint at an interesting tentative conclusion: high nonlinear shear rates can potentially invert enhancement in viscosity and moduli normally observed near rigid attractive interfaces. This tentative finding may have implications for high-rate deformation of polymeric nanocomposites and evidently warrants additional attention.

Conclusions

These findings provide new insight into the relationship between interfacial gradients in segmental dynamics and interfacial gradients in chain motion and viscosity. First, they indicate that gradients in viscosity exhibit the same qualitative features that have been observed for segmental relaxation: near-interface chain relaxation and viscosity obey a fractional power law decoupling relation with bulk viscosity; the "decoupling exponent" or activation barrier truncation factor in this relation exhibits an exponential decay with increasing distance from the interface; the viscosity and chain relaxation times themselves consequently recovers its bulk value in a double-exponential manner with distance from the interface. These results suggest that alterations in viscosity, chain relaxation, and segmental relaxation near rigid substrates all emanate from the same underlying mechanism.

A recent perspective co-authored by one of us recently reviewed the state of theoretical understanding of segmental relaxation time gradients, concluding that the Elastically Cooperative Nonlinear Langevin Equation theory of glass formation presently predicts the largest portion of the phenomenology of these gradients. Within this theory, near interface alterations in dynamics are driven by a combination of altered caging constraints near an interface and alterations in collective far-field elastic contribution to the barrier to relaxation. Our findings for *segmental* dynamics near a substrate are in remarkable accord with the predictions of this theory[28,87], including qualitative predictions of fractional power law decoupling and the spatial form of the gradient. Moreover, there appears to be a good degree of *quantitative* agreement between simulation and theory: our simulations report a near-substrate gradient range in segmental ln(τ) in the vicinity of 2σ, in reasonable agreement with theory[87]. Moreover, as in the theory this range is reduced relative to prior reports

of the range of gradients in this quantity at a free surface. The present results indicate that this same elasticity and caging based mechanism likely underpins alterations in near-interface viscosity at a qualitative level, although clearly further theoretical work is needed to quantitatively extend these predictions to chain-scale relaxation and viscous response.

From a practical standpoint, these findings thus indicate that measurements of near-surface perturbation in viscous response can be interpreted as *qualitatively to semiquantitatively* reporting on shifts in T_g and segmental dynamics. However, we find that shifts in viscosity are *quantitatively* weaker than underlying shifts in segmental dynamics. This difference results at least in part from the difference in the *bulk* temperature dependence of viscosity vs segmental relaxation time – a connection resulting from the convolution of an underlying activation barrier gradient with the bulk temperature dependence of dynamics to yield the gradient in relaxation time. In many polymers, viscosity near T_g is observed to exhibit a weaker temperature dependence than segmental dynamics. Weak viscosity gradients – relative to segmental time gradients – should thus generally represent a unique feature of polymers resulting from this bulk level segment/chain decoupling.

Moreover, these results provide a predictive rule regarding the extent of decoupling between viscosity and segmental relaxation time gradients. Specifically, the extent of bulk decoupling between segmental dynamics and viscosity can be quantified by a 'decoupling exponent' that is available for a number of polymers[58] or can readily be obtained from viscosity and segmental relaxation time data. These findings suggest that higher values of this exponent will tend to correlate with weaker viscosity gradients *relative* to the segmental relaxation time gradient, given equal bulk relaxation time temperature dependences. This may provide a useful design rule for obtaining relative uniform viscosity near interfaces. This tendency may also be overlaid with effects emanating from variations in the onset timescale of interfacial alterations between distinct relaxation function, which may become more important as chain stiffness is increased[30]. At the same time, evidence also suggests that chain relaxation exhibits less polymer-to-polymer variation in fragility of glass formation than does segmental relaxation[58]; this may suggest that polymer interfacial gradients in viscosity may be less sensitive to chemistry than are gradients in segmental dynamics. Most broadly, these results indicate that surface rheology measurements should *not* be interpreted as *quantitatively* reporting in a simple way on the precise magnitude of underlying T_g and segmental relaxation time gradients.

These observations may be related to prior results pointing towards a correlation of the strength of alterations in T_g in thin films with a material's bulk *fragility* of glass formation – a measure of the strength of the temperature dependence of dynamics near T_g.[20] However, when comparing distinct chemistries, it is even likely that additional factors, such as chemical dependences of the underlying strength of the barrier gradients or of the onset of these effects[30], may be involved, potentially explaining why this relationship is nonuniversal[76].

We additionally probe interfacial alterations in complex modulus that underlie the surface viscosity gradient. Results indicate that near-surface material develops mechanical features of 'glassiness' (i.e. emergence of a well-defined glassy modulus) sooner than does bulk-like material, supporting the intuitive notion that near-substrate material is 'glassier' than bulk material. Results also tentatively suggest that high shear rates can suppress or even invert this interfacial gradient, with potential implications for high-rate deformation of interfacially-rich materials.

Finally, we emphasize that our present findings are limited to low molecular weight polymers. The chains we simulate here have an end to end distance of order similar to the exponential decay range of the surface gradient in segmental relaxation times. It is entirely possible that longer-range connectivity effects change the picture in higher molecular weight chains. Similarly, our chains are unentangled, and entanglement effects in longer chains may again alter the picture – such a scenario is supported by the bubble inflation studies of McKenna and coworkers on film comprised of entangled polymers[48–51]. Our findings are also restricted to relaxation near substrates where T_g is enhanced; it is conceivable that the situation may qualitatively change near free surfaces or repulsive interfaces where T_g is suppressed.

Overall, our findings indicate that the bulk-based intuition that viscosity quantitatively tracks whole chain relaxation in polymers is evidently incomplete near an interface. This is a natural consequence of the presence of an organized gradient in segmental mobility, which violates a basic assumption of the Rouse model. Fundamentally, these findings thus highlight the need for a new generalization of the Rouse theory accounting for gradients in segmental mobility. Such a generalization may be a logical next step of the recently developed Heterogeneous Rouse Model[61]. Practically, these findings emphasize that nanostructured materials exhibiting alterations in T_g should be expected to exhibit accompanying shifts in viscosity and dissipation behavior, albeit with a weaker magnitude. These effects can be expected to play an important role in classes of materials including polymer nanocomposites and filled elastomers. A generalization of the Rouse model accounting for these gradients, enabling quantitative prediction of shifts in viscosity in nanostructured materials based upon T_g measurements, could thus have substantial implications for the design of these materials. Such an extension could also provide a foundation for an understanding of the likely more complex near-interface effects that may arise as chain-entanglement effects begin to play a role at even higher molecular weights.

ASSOCIATED CONTENT

AUTHOR INFORMATION

Corresponding Author

* dssimmons@usf.edu

Author Contributions

The manuscript was written through contributions of all authors. All authors have given approval to the final version of the manuscript.

ACKNOWLEDGMENT

T. Rahman acknowledges support from the Center for Tire Research, a National Science Foundation (NSF) Industry/University Cooperative Research Center supported by NSF award 1160982. D. Simmons acknowledges support from the National Science Foundation under Grant No. CBET1705738.

REFERENCES

(1) Schweizer, K. S.; Simmons, D. S. Progress towards a Phenomenological Picture and Theoretical Understanding of Glassy Dynamics and Vitrification near Interfaces and under Nanoconfinement. *J. Chem. Phys.* **2019**, *151*, 240901.

(2) Ediger, M. D.; Forrest, J. A. Dynamics near Free Surfaces and the Glass Transition in Thin Polymer Films: A View to the Future. *Macromolecules* **2014**, *47* (2), 471–478. https://doi.org/10.1021/ma4017696.

(3) McKenna, G. B. Ten (or More) Years of Dynamics in Confinement: Perspectives for 2010. *Eur. Phys. J. Spec. Top.* **2010**, *189* (1), 285–302.

(4) Baschnagel, J.; Varnik, F. Computer Simulations of Supercooled Polymer Melts in the Bulk and in Confined Geometry. *J. Phys. Condens. Matter* **2005**, *17* (32), R851–R953. https://doi.org/10.1088/0953-8984/17/32/R02.

(5) Forrest, J. A.; Dalnoki-Veress, K. The Glass Transition in Thin Polymer Films. *Adv. Colloid Interface Sci.* **2001**, *94* (1–3), 167–195. https://doi.org/10.1016/S0001-8686(01)00060-4.

(6) Keddie, J. L.; Jones, R. A. L.; Cory, R. A. Size-Dependent Depression of the Glass Transition Temperature in Polymer Films. *Europhys. Lett.* **1994**, *27* (1), 59–64. https://doi.org/10.1209/0295-5075/27/1/011.

(7) Ellison, C. J.; Torkelson, J. M. The Distribution of Glass-Transition Temperatures in Nanoscopically Confined Glass Formers. *Nat. Mater.* **2003**, *2* (10), 695–700. https://doi.org/10.1038/nmat980.

(8) Lee, J.; Mangalara, J. H.; Simmons, D. S. Correspondence between the Rigid Amorphous Fraction and Nanoconfinement Effects on Glass Formation. *J. Polym. Sci. Part B Polym. Phys.* **2017**, *55* (12), 907–918. https://doi.org/10.1002/polb.24324.

(9) Wunderlich, B. Reversible Crystallization and the Rigid–Amorphous Phase in Semicrystalline Macromolecules. *Prog. Polym. Sci.* **2003**, *28* (3), 383–450. https://doi.org/10.1016/S0079-6700(02)00085-0.

(10) Ruan, D.; Simmons, D. S. Glass Formation near Covalently Grafted Interfaces: Ionomers as a Model Case. *Macromolecules* **2015**, *48* (7), 2313–2323. https://doi.org/10.1021/acs.macromol.5b00025.

(11) Ruan, D.; Simmons, D. S. Roles of Chain Stiffness and Segmental Rattling in Ionomer Glass Formation. *J. Polym. Sci. Part B Polym. Phys.* **2015**, *53* (20), 1458–1469. https://doi.org/10.1002/polb.23788.

(12) Eisenberg, A.; Hird, B.; Moore, R. B. A New Multiplet-Cluster Model for the Morphology of Random Ionomers. *Macromolecules* **1990**, *23* (18), 4098–4107. https://doi.org/10.1021/ma00220a012.

(13) Slimani, M. Z.; Moreno, A. J.; Colmenero, J. Heterogeneity of the Segmental Dynamics in Lamellar Phases of Diblock Copolymers. *Macromolecules* **2011**, *44* (17), 6952–6961. https://doi.org/10.1021/ma200470a.

(14) Simmons, D. S. An Emerging Unified View of Dynamic Interphases in Polymers. *Macromol. Chem. Phys.* **2016**, *217* (2), 137–148. https://doi.org/10.1002/macp.201500284.

(15) Slimani, M. Z.; Moreno, A. J.; Colmenero, J. Heterogeneity of the Segmental Dynamics in Cylindrical and Spherical Phases of Diblock Copolymers. *Macromolecules* **2012**, *45* (21), 8841–8852. https://doi.org/10.1021/ma301388j.

(16) Slimani, M. Z.; Moreno, A. J.; Rossi, G.; Colmenero, J. Dynamic Heterogeneity in Random and Gradient Copolymers: A Computational Investigation. *Macromolecules* **2013**, *46* (12), 5066–5079. https://doi.org/10.1021/ma400577d.

(17) Roth, C. B.; Torkelson, J. M. Selectively Probing the Glass Transition Temperature in Multilayer Polymer Films: Equivalence of Block Copolymers and Multilayer Films of Different Homopolymers. *Macromolecules* **2007**, *40* (9), 3328–3336. https://doi.org/10.1021/ma070162g.

(18) Wang, J.; McKenna, G. B. A Novel Temperature-Step Method to Determine the Glass Transition Temperature of Ultrathin Polymer Films by Liquid Dewetting. *J. Polym. Sci. Part B Polym. Phys.* **2013**, *51* (18), 1343–1349.

(19) Merling, W. L.; Mileski, J. B.; Douglas, J. F.; Simmons, D. S. The Glass Transition of a Single Macromolecule. *Macromolecules* **2016**, *49* (19), 7597–7604. https://doi.org/10.1021/acs.macromol.6b01461.

(20) Evans, C. M.; Deng, H.; Jager, W. F.; Torkelson, J. M. Fragility Is a Key Parameter in Determining the Magnitude of Tg-Confinement Effects in Polymer Films. *Macromolecules* **2013**, *46* (15), 6091–6103.

(21) Peter, S.; Meyer, H.; Baschnagel, J. Thickness-Dependent Reduction of the Glass-Transition Temperature in Thin Polymer Films with a Free Surface. *J. Polym. Sci. Part B-Polym. Phys.* **2006**, *44* (20), 2951–2967. https://doi.org/10.1002/polb.20924.

(22) Scheidler, P.; Kob, W.; Binder, K. Cooperative Motion and Growing Length Scales in Supercooled Confined Liquids. *Europhys. Lett.* **2002**, *59* (5), 701–707. https://doi.org/10.1209/epl/i2002-00182-9.

(23) Scheidler, P.; Kob, W.; Binder, K. The Relaxation Dynamics of a Confined Glassy Simple Liquid. *Eur.*

Phys. J. E **2003**, *12* (1), 5–9. https://doi.org/10.1140/epje/i2003-10041-7.

(24) Scheidler, P.; Kob, W.; Binder, K. The Relaxation Dynamics of a Supercooled Liquid Confined by Rough Walls. *J. Phys. Chem. B* **2004**, *108* (21), 6673–6686. https://doi.org/10.1021/jp036593s.

(25) Kob, W.; Roldán-Vargas, S.; Berthier, L. Non-Monotonic Temperature Evolution of Dynamic Correlations in Glass-Forming Liquids. *Nat. Phys.* **2012**, *8* (2), 164–167. https://doi.org/10.1038/nphys2133.

(26) Hocky, G. M.; Berthier, L.; Kob, W.; Reichman, D. R. Crossovers in the Dynamics of Supercooled Liquids Probed by an Amorphous Wall. *Phys. Rev. E* **2014**, *89* (5), 052311. https://doi.org/10.1103/PhysRevE.89.052311.

(27) Kob, W.; Coslovich, D. Nonlinear Dynamic Response of Glass-Forming Liquids to Random Pinning. *Phys. Rev. E* **2014**, *90* (5), 052305. https://doi.org/10.1103/PhysRevE.90.052305.

(28) Phan, A. D.; Schweizer, K. S. Theory of the Spatial Transfer of Interface-Nucleated Changes of Dynamical Constraints and Its Consequences in Glass-Forming Films. *J. Chem. Phys.* **2019**, *150* (4), 044508. https://doi.org/10.1063/1.5079250.

(29) Diaz-Vela, D.; Hung, J.-H.; Simmons, D. S. Temperature-Independent Rescaling of the Local Activation Barrier Drives Free Surface Nanoconfinement Effects on Segmental-Scale Translational Dynamics near Tg. *ACS Macro Lett.* **2018**, *7* (11), 1295–1301. https://doi.org/10.1021/acsmacrolett.8b00695.

(30) Vela, D.; Ghanekarade, A.; Simmons, D. S. Probing the Metrology and Chemistry Dependences of the Onset Condition of Strong "Nanoconfinement" Effects on Dynamics. *Macromolecules* **2020**, *53* (11), 4158–4171. https://doi.org/10.1021/acs.macromol.9b02693.

(31) Mirigian, S.; Schweizer, K. S. Elastically Cooperative Activated Barrier Hopping Theory of Relaxation in Viscous Fluids. I. General Formulation and Application to Hard Sphere Fluids. *J. Chem. Phys.* **2014**, *140* (19), 194506. https://doi.org/10.1063/1.4874842.

(32) Mirigian, S.; Schweizer, K. S. Elastically Cooperative Activated Barrier Hopping Theory of Relaxation in Viscous Fluids. II. Thermal Liquids. *J. Chem. Phys.* **2014**, *140* (19), 194507. https://doi.org/10.1063/1.4874843.

(33) White, R. P.; Lipson, J. E. G. To Understand Film Dynamics Look to the Bulk. *Phys. Rev. Lett.* **2020**, *125* (5), 058002. https://doi.org/10.1103/PhysRevLett.125.058002.

(34) Servantie, J.; Müller, M. Temperature Dependence of the Slip Length in Polymer Melts at Attractive Surfaces. *Phys. Rev. Lett.* **2008**, *101* (2), 026101. https://doi.org/10.1103/PhysRevLett.101.026101.

(35) Yang, Z.; Fujii, Y.; Lee, F. K.; Lam, C.-H.; Tsui, O. K. C. Glass Transition Dynamics and Surface Layer Mobility in Unentangled Polystyrene Films. *Science* **2010**, *328* (5986), 1676–1679. https://doi.org/10.1126/science.1184394.

(36) Wang, S.; Yang, S.; Lee, J.; Akgun, B.; Wu, D. T.; Foster, M. D. Anomalous Surface Relaxations of Branched-Polymer Melts. *Phys. Rev. Lett.* **2013**, *111* (6), 068303. https://doi.org/10.1103/PhysRevLett.111.068303.

(37) Chai, Y.; Salez, T.; McGraw, J. D.; Benzaquen, M.; Dalnoki-Veress, K.; Raphaël, E.; Forrest, J. A. A Direct Quantitative Measure of Surface Mobility in a Glassy Polymer. *Science* **2014**, *343* (6174), 994–999. https://doi.org/10.1126/science.1244845.

(38) Fakhraai, Z.; Forrest, J. A. Measuring the Surface Dynamics of Glassy Polymers. *Science* **2008**, *319* (5863), 600–604.

(39) Chowdhury, M.; Guo, Y.; Wang, Y.; Merling, W. L.; Mangalara, J. H.; Simmons, D. S.; Priestley, R. D. Spatially Distributed Rheological Properties in Confined Polymers by Noncontact Shear. *J. Phys. Chem. Lett.* **2017**, *8* (6), 1229–1234. https://doi.org/10.1021/acs.jpclett.7b00214.

(40) Daley, C. R.; Fakhraai, Z.; Ediger, M. D.; Forrest, J. A. Comparing Surface and Bulk Flow of a Molecular Glass Former. *Soft Matter* **2012**, *8* (7), 2206–2212. https://doi.org/10.1039/C2SM06826E.

(41) Teichroeb, J. H.; Forrest, J. A. Direct Imaging of Nanoparticle Embedding to Probe Viscoelasticity of Polymer Surfaces. *Phys. Rev. Lett.* **2003**, *91* (1), 016104. https://doi.org/10.1103/PhysRevLett.91.016104.

(42) Ilton, M.; Qi, D.; Forrest, J. A. Using Nanoparticle Embedding to Probe Surface Rheology and the Length Scale of Surface Mobility in Glassy Polymers. *Macromolecules* **2009**, *42* (18), 6851–6854. https://doi.org/10.1021/ma901057b.

(43) Dannenberg, E. M. Bound Rubber and Carbon Black Reinforcement. *Rubber Chem. Technol.* **1986**, *59* (3), 512–524. https://doi.org/10.5254/1.3538213.

(44) Wang, M.-J. Effect of Polymer-Filler and Filler-Filler Interactions on Dynamic Properties of Filled Vulcanizates. *Rubber Chem. Technol.* **1998**, *71* (3), 520–589. https://doi.org/10.5254/1.3538492.

(45) Heinrich, G.; Klüppel, M.; Vilgis, T. A. Reinforcement of Elastomers. *Curr. Opin. Solid State Mater. Sci.* **2002**, *6* (3), 195–203. https://doi.org/10.1016/S1359-0286(02)00030-X.

(46) Pryamitsyn, V.; Ganesan, V. Origins of Linear Viscoelastic Behavior of Polymer–Nanoparticle Composites. *Macromolecules* **2006**, *39* (2), 844–856. https://doi.org/10.1021/ma0518412.

(47) Kumar, S. K.; Benicewicz, B. C.; Vaia, R. A.; Winey, K. I. 50th Anniversary Perspective: Are Polymer Nanocomposites Practical for Applications? *Macromolecules* **2017**, *50* (3), 714–731. https://doi.org/10.1021/acs.macromol.6b02330.

(48) O'Connell, P. A.; McKenna, G. B. A Novel Nano-Bubble Inflation Method for Determining the Viscoelastic Properties of Ultrathin Polymer Films. *Scanning* **2008**, *30* (2), 184–196. https://doi.org/10.1002/sca.20088.

(49) O'Connell, P. A.; Hutcheson, S. A.; McKenna, G. B. Creep Behavior of Ultra-Thin Polymer Films. *J. Polym. Sci. Part B Polym. Phys.* **2008**, *46* (18), 1952–1965. https://doi.org/10.1002/polb.21531.

(50) Li, X.; McKenna, G. B. Ultrathin Polymer Films: Rubbery Stiffening, Fragility, and Tg Reduction. *Macromolecules* **2015**, *48* (17), 6329–6336. https://doi.org/10.1021/acs.macromol.5b01263.

(51) Yoon, H.; McKenna, G. B. Dynamic and Temperature Dependent Response of Physical Vapor Deposited Se in Freely Standing Nanometric Thin Films. *J. Chem. Phys.* **2016**, *144* (18), 184501. https://doi.org/10.1063/1.4948322.

(52) Si, L.; Massa, M. V.; Dalnoki-Veress, K.; Brown, H. R.; Jones, R. A. L. Chain Entanglement in Thin Freestanding Polymer Films. *Phys. Rev. Lett.* **2005**, *94* (12), 127801. https://doi.org/10.1103/PhysRevLett.94.127801.

(53) Brown, H. R.; Russell, T. P. Entanglements at Polymer Surfaces and Interfaces. *Macromolecules* **1996**, *29* (2), 798–800. https://doi.org/10.1021/ma951123k.

(54) Varnik, F.; Binder, K. Shear Viscosity of a Supercooled Polymer Melt via Nonequilibrium Molecular Dynamics Simulations. *J. Chem. Phys.* **2002**, *117* (13), 6336–6349. https://doi.org/10.1063/1.1503770.

(55) Priezjev, N. V. Shear Rate Threshold for the Boundary Slip in Dense Polymer Films. *Phys. Rev. E* **2009**, *80* (3), 031608. https://doi.org/10.1103/PhysRevE.80.031608.

(56) Lam, C.-H.; Tsui, O. K. C. Crossover to Surface Flow in Supercooled Unentangled Polymer Films. *Phys. Rev. E* **2013**, *88* (4), 042604. https://doi.org/10.1103/PhysRevE.88.042604.

(57) Rubinstein, M. *Polymer Physics*; Oxford University Press, 2003.

(58) Sokolov, A. P.; Schweizer, K. S. Resolving the Mystery of the Chain Friction Mechanism in Polymer Liquids. *Phys. Rev. Lett.* **2009**, *102* (24), 248301. https://doi.org/10.1103/PhysRevLett.102.248301.

(59) Ngai, K. L.; Plazek, D. J.; Roland, C. M. Comment on ``Resolving the Mystery of the Chain Friction Mechanism in Polymer Liquids''. *Phys. Rev. Lett.* **2009**, *103* (15), 159801. https://doi.org/10.1103/PhysRevLett.103.159801.

(60) Sokolov, A. P.; Schweizer, K. S. Sokolov and Schweizer Reply: *Phys. Rev. Lett.* **2009**, *103* (15), 159802. https://doi.org/10.1103/PhysRevLett.103.159802.

(61) Hung, J.-H.; Mangalara, J. H.; Simmons, D. S. Heterogeneous Rouse Model Predicts Polymer Chain Translational Normal Mode Decoupling. *Macromolecules* **2018**, *51* (8), 2887–2898. https://doi.org/10.1021/acs.macromol.8b00135.

(62) Loring, R. F. A Model of Relaxation in Supercooled Polymer Melts. *J. Chem. Phys.* **1998**, *108* (5), 2189–2196.

(63) Ngai, K. L.; Plazek, D. J. A Quantitative Explanation of the Difference in the Temperature Dependences of the Viscoelastic Softening and Terminal Dispersions of Linear Amorphous Polymers. *J. Polym. Sci. Part B Polym. Phys.* **1986**, *24* (3), 619–632. https://doi.org/10.1002/polb.1986.090240310.

(64) Plazek, D. J.; Zheng, X. D.; Ngai, K. L. Viscoelastic Properties of Amorphous Polymers. I. Different Temperature Dependences of Segmental Relaxation and Terminal Dispersion. *Macromolecules* **1992**, *25* (19), 4920–4924. https://doi.org/10.1021/ma00045a016.

(65) Plazek, D. J.; Bero, C. A.; Neumeister, S.; Floudas, G.; Fytas, G.; Ngai, K. L. Viscoelastic Properties of Amorphous Polymers 3: Low Molecular Weight Poly(Methylphenylsiloxane). *Colloid Polym. Sci.* **1994**, *272* (11), 1430–1438. https://doi.org/10.1007/BF00654173.

(66) Roland, C. M.; Ngai, K. L.; Plazek, D. J. Modes of Molecular Motion in Low Molecular Weight Polystyrene. *Macromolecules* **2004**, *37* (18), 7051–7055. https://doi.org/10.1021/ma049573c.

(67) Lin, Y.-H. Glass Transition-Related Thermorheological Complexity in Polystyrene Melts. *J. Phys. Condens. Matter* **2007**, *19* (46), 466101. https://doi.org/10.1088/0953-8984/19/46/466101.

(68) Grest, G. S.; Kremer, K. Molecular Dynamics Simulation for Polymers in the Presence of a Heat Bath. *Phys. Rev. A* **1986**, *33* (5), 3628.

(69) Riggleman, R. A.; Yoshimoto, K.; Douglas, J. F.; de Pablo, J. J. Influence of Confinement on the Fragility of Antiplasticized and Pure Polymer Films. *Phys. Rev. Lett.* **2006**, *97* (4), 045502.

(70) Shavit, A.; Riggleman, R. A. Influence of Backbone Rigidity on Nanoscale Confinement Effects in Model Glass-Forming Polymers. *Macromolecules* **2013**. https://doi.org/10.1021/ma400210w.

(71) Baschnagel, J.; Varnik, F. Computer Simulations of Supercooled Polymer Melts in the Bulk and in Confined Geometry. *J. Phys. Condens. Matter* **2005**, *17* (32), R851–R953. https://doi.org/10.1088/0953-8984/17/32/R02.

(72) Lang, R. J.; Simmons, D. S. Interfacial Dynamic Length Scales in the Glass Transition of a Model Freestanding Polymer Film and Their Connection to Cooperative Motion. *Macromolecules* **2013**, *46* (24), 9818–9825. https://doi.org/10.1021/ma401525q.

(73) Lang, R. J.; Merling, W. L.; Simmons, D. S. Combined Dependence of Nanoconfined Tg on Interfacial Energy and Softness of Confinement. *ACS Macro Lett.* **2014**, *3* (8), 758–762. https://doi.org/10.1021/mz500361v.

(74) Marvin, M. D.; Lang, R. J.; Simmons, D. S. Nanoconfinement Effects on the Fragility of Glass Formation of a Model Freestanding Polymer Film. *Soft Matter* **2014**, *10* (18), 3166–3170. https://doi.org/10.1039/C3SM53160K.

(75) Mangalara, J. H.; Marvin, M. D.; Simmons, D. S. Three-Layer Model for the Emergence of Ultrastable Glasses from the Surfaces of Supercooled Liquids. *J. Phys. Chem. B* **2016**, *120* (21), 4861–4865. https://doi.org/10.1021/acs.jpcb.6b04736.

(76) Mangalara, J. H.; Marvin, M. D.; Wiener, N. R.; Mackura, M. E.; Simmons, D. S. Does Fragility of Glass Formation Determine the Strength of Tg-Nanoconfinement Effects? *J. Chem. Phys.* **2017**, *146* (10), 104902. https://doi.org/10.1063/1.4976521.

(77) Mangalara, J. H.; Mackura, M. E.; Marvin, M. D.; Simmons, D. S. The Relationship between Dynamic and Pseudo-Thermodynamic Measures of the Glass Transition Temperature in Nanostructured Materials. *J. Chem. Phys.* **2017**, *146* (20), 203316. https://doi.org/10.1063/1.4977520.

(78) Hanakata, P. Z.; Douglas, J. F.; Starr, F. W. Interfacial Mobility Scale Determines the Scale of Collective Motion and Relaxation Rate in Polymer Films. *Nat. Commun.* **2014**, *5*, 4163. https://doi.org/10.1038/ncomms5163.

(79) Hanakata, P. Z.; Douglas, J. F.; Starr, F. W. Local Variation of Fragility and Glass Transition Temperature of Ultra-Thin Supported Polymer Films. *J. Chem. Phys.* **2012**, *137* (24), 244901. https://doi.org/doi:10.1063/1.4772402.

(80) Mackura, M. E.; Simmons, D. S. Enhancing Heterogenous Crystallization Resistance in a Bead-Spring Polymer Model by Modifying Bond Length. *J. Polym. Sci. Part B Polym. Phys.* **2013**. https://doi.org/10.1002/polb.23398.

(81) Humphrey, W.; Dalke, A.; Schulten, K. VMD – Visual Molecular Dynamics. *J. Mol. Graph.* **1996**, *14*, 33–38.

(82) Hung, J.-H.; Patra, T. K.; Meenakshisundaram, V.; Mangalara, J. H.; Simmons, D. S. Universal Localization Transition Accompanying Glass Formation: Insights from Efficient Molecular Dynamics Simulations of Diverse Supercooled Liquids. *Soft Matter* **2019**, *15* (6), 1223–1242. https://doi.org/10.1039/C8SM02051E.

(83) Plimpton, S. Fast Parallel Algorithms for Short-Range Molecular Dynamics. *J. Comput. Phys.* **1995**, *117* (1), 1–19. https://doi.org/10.1006/jcph.1995.1039.

(84) Kremer, K.; Grest, G. S. Dynamics of Entangled Linear Polymer Melts: A Molecular-dynamics Simulation. *J. Chem. Phys.* **1990**, *92* (8), 5057–5086. https://doi.org/10.1063/1.458541.

(85) Mangalara, J. H.; Simmons, D. S. Tuning Polymer Glass Formation Behavior and Mechanical Properties with Oligomeric Diluents of Varying Stiffness. *ACS Macro Lett.* **2015**, *4* (10), 1134–1138. https://doi.org/10.1021/acsmacrolett.5b00635.

(86) Forrest, J. A. What Can We Learn about a Dynamical Length Scale in Glasses from Measurements of Surface Mobility? *J. Chem. Phys.* **2013**, *139* (8), 084702. https://doi.org/10.1063/1.4818989.

(87) Phan, A. D.; Schweizer, K. S. Theory of Spatial Gradients of Relaxation, Vitrification Temperature and Fragility of Glass-Forming Polymer Liquids Near Solid Substrates. *ACS Macro Lett.* **2020**, *9* (4), 448–453. https://doi.org/10.1021/acsmacrolett.0c00006.

(88) Torres, J. M.; Wang, C.; Coughlin, E. B.; Bishop, J. P.; Register, R. A.; Riggleman, R. A.; Stafford, C. M.; Vogt, B. D. Influence of Chain Stiffness on Thermal and Mechanical Properties of Polymer Thin Films. *Macromolecules* **2011**, *44* (22), 9040–9045. https://doi.org/10.1021/ma201482b.

(89) Plazek, D. J. Temperature Dependence of the Viscoelastic Behavior of Polystyrene. *J. Phys. Chem.* **1965**, *69* (10), 3480–3487. https://doi.org/10.1021/j100894a039.

(90) Plazek, D. J. The Temperature Dependence of the Viscoelastic Softening and Terminal Dispersions of Linear Amorphous Polymers. *J. Polym. Sci. Polym. Phys. Ed.* **1982**, *20* (4), 729–742. https://doi.org/10.1002/pol.1982.180200414.

(91) Ding, Y.; Sokolov, A. P. Breakdown of Time–Temperature Superposition Principle and Universality of Chain Dynamics in Polymers. *Macromolecules* **2006**, *39* (9), 3322–3326. https://doi.org/10.1021/ma052607b.

(92) Sokolov, A. P.; Hayashi, Y. Breakdown of Time–Temperature Superposition: From Experiment to the Coupling Model and Beyond. *J. Non-Cryst. Solids* **2007**, *353* (41–43), 3838–3844. https://doi.org/10.1016/j.jnoncrysol.2007.02.063.

(93) Ngai, K. L.; Plazek, D. J. Identification of Different Modes of Molecular Motion in Polymers That Cause Thermorheological Complexity. *Rubber Chem. Technol.* **1995**, *68* (3), 376–434. https://doi.org/10.5254/1.3538749.

(94) Santangelo, P. G.; Ngai, K. L.; Roland, C. M. Temperature Dependence of Relaxation in Polypropylene and Poly(Ethylene-Co-Propylene). *Macromolecules* **1996**, *29* (10), 3651–3653. https://doi.org/10.1021/ma9515310.

(95) Plazek, D. L.; Plazek, D. J. Viscoelastic Behavior of Atactic Polypropylene. *Macromolecules* **1983**, *16* (9), 1469–1475. https://doi.org/10.1021/ma00243a011.

(96) Inoue, T.; Onogi, T.; Yao, M.-L.; Osaki, K. Viscoelasticity of Low Molecular Weight Polystyrene. Separation of Rubbery and Glassy Components. *J. Polym. Sci. Part B Polym. Phys.* **1999**, *37* (4), 389–397. https://doi.org/10.1002/(SICI)1099-0488(19990215)37:4<389::AID-POLB12>3.0.CO;2-G.

(97) Baglay, R. R.; Roth, C. B. Local Glass Transition Temperature $T_g(z)$ of Polystyrene next to Different Polymers: Hard vs. Soft Confinement. *J. Chem. Phys.* **2017**, *146* (20), 203307. https://doi.org/10.1063/1.4975168.

(98) Baglay, R. R.; Roth, C. B. Communication: Experimentally Determined Profile of Local Glass

Transition Temperature across a Glassy-Rubbery Polymer Interface with a Tg Difference of 80 K. *J. Chem. Phys.* **2015**, *143* (11), 111101. https://doi.org/10.1063/1.4931403.

(99) Evans, C. M.; Kim, S.; Roth, C. B.; Priestley, R. D.; Broadbelt, L. J.; Torkelson, J. M. Role of Neighboring Domains in Determining the Magnitude and Direction of Tg-Confinement Effects in Binary, Immiscible Polymer Systems. *Polymer* **2015**, *80*, 180–187. https://doi.org/10.1016/j.polymer.2015.10.059.

SYNOPSIS TOC